THE FASEB JOURNAL • RESEARCH • www.fasebj.org

N-acetylaspartate availability is essential for juvenile survival on fat-free diet and determines metabolic health

Dina C. Hofer,[*,†] Gabriel Zirkovits,[*] Helmut J. Pelzmann,[*,‡] Katharina Huber,[*,§] Ariane R. Pessentheiner,[*,¶] Wenmin Xia,[*] Kyosuke Uno,[‖] Toh Miyazaki,[‖] Kanta Kon,[#] Hiroshi Tsuneki,[#] Tobias Pendl,[**] Wael Al Zoughbi,[††] Corina T. Madreiter-Sokolowski,[‡‡] Gert Trausinger,[§§] Mahmoud Abdellatif,[¶¶] Gabriele Schoiswohl,[‖‖] Renate Schreiber,[‖‖] Tobias Eisenberg,[,##] Christoph Magnes,[§§] Simon Sedej,[¶¶,##] Matthias Eckhardt,[***] Masakiyo Sasahara,[†††] Toshiyasu Sasaoka,[#] Atsumi Nitta,[‖] Gerald Hoefler,[††] Wolfgang F. Graier,[‡‡,##] Dagmar Kratky,[‡‡,##] Johan Auwerx,[†] and Juliane G. Bogner-Strauss[*,##,1]**

[*]Institute of Biochemistry, Graz University of Technology, Graz, Austria; [†]Laboratory of Integrative and Systems Physiology, Institute of Bioengineering, École Polytechnique Fédérale de Lausanne, Lausanne, Switzerland; [‡]Fresenius Kabi Austria GmbH, Graz, Austria; [§]Center for Integrative Genomics, University of Lausanne, Lausanne, Switzerland; [¶]Department of Medicine, University of California–San Diego, La Jolla, California, USA; [‖]Department of Pharmaceutical Therapy and Neuropharmacology, Faculty of Pharmaceutical Sciences, Graduate School of Medicine and Pharmaceutical Sciences, [#]Department of Clinical Pharmacology, and [†††]Department of Pathology, University of Toyama, Toyama, Japan; [**]Institute of Molecular Biosciences, NAWI Graz, and [‖‖]Institute of Molecular Biosciences, University of Graz, Graz, Austria; [††]Institute of Pathology, [‡‡]Gottfried Schatz Research Center, and [¶¶]Department of Cardiology, Medical University of Graz, Graz, Austria; [§§]Joanneum Research, HEALTH–Institute for Biomedicine and Health Sciences, Graz, Austria; [##]BioTechMed-Graz, Graz, Austria; and [***]Institute of Biochemistry and Molecular Biology, University of Bonn, Bonn, Germany

ABSTRACT: ***N*-acetylaspartate (NAA) is synthesized by aspartate *N*-acetyltransferase (gene: *Nat8l*) from acetyl–coenzyme A and aspartate. In the brain, NAA is considered an important energy metabolite for lipid synthesis. However, the role of NAA in peripheral tissues remained elusive. Therefore, we characterized the metabolic phenotype of knockout (ko) and adipose tissue–specific (ako) *Nat8l*-ko mice as well as NAA-supplemented mice on various diets. We identified an important role of NAA availability in the brain during adolescence, as 75% of *Nat8l*-ko mice died on fat-free diet (FFD) after weaning but could be rescued by NAA supplementation. In adult life, NAA deficiency promotes a beneficial metabolic phenotype, as *Nat8l*-ko and *Nat8l*-ako mice showed reduced body weight, increased energy expenditure, and improved glucose tolerance on chow, high-fat, and FFDs. Furthermore, *Nat8l*-deficient adipocytes exhibited increased mitochondrial respiration, ATP synthesis, and an induction of browning. Conversely, NAA-treated wild-type mice showed reduced adipocyte respiration and lipolysis and increased *de novo* lipogenesis, culminating in reduced energy expenditure, glucose tolerance, and insulin sensitivity. Mechanistically, our data point to a possible role of NAA as modulator of pancreatic insulin secretion and suggest NAA as a critical energy metabolite for adipocyte and whole-body energy homeostasis.—Hofer, D. C., Zirkovits, G., Pelzmann, H. J., Huber, K., Pessentheiner, A. R., Xia, W., Uno, K., Miyazaki, T., Kon, K., Tsuneki, H., Pendl, T., Al Zoughbi, W., Madreiter-Sokolowski, C. T., Trausinger, G., Abdellatif, M., Schoiswohl, G., Schreiber, R., Eisenberg, T., Magnes, C., Sedej, S., Eckhardt, M., Sasahara, M., Sasaoka, T., Nitta, A., Hoefler, G., Graier, W. F., Kratky, D., Auwerx, J., Bogner-Strauss, J. G. *N*-acetylaspartate availability is essential for juvenile survival on fat-free diet and determines metabolic health. FASEB J. 33, 13808–13824 (2019). www.fasebj.org**

KEY WORDS: NAA · acetyl-CoA · energy homeostasis · adipose tissue · insulin secretion

ABBREVIATIONS: ACC, acetyl-CoA carboxylase; *Acly*, ATP citrate lyase; ACTb, β-actin; ako, AT-specific; Asp-NAT, aspartate *N*-acetyltransferase; ASPA, aspartoacylase; AT, adipose tissue; ATGL, adipose TG lipase; BAT, brown AT; BCA, bicinchoninic acid assay; BSA, bovine serum albumin; CD, chow diet; CL, CL-316,243; DG, diglyceride; DNL, *de novo* lipogenesis; ECG, electrocardiography; eWAT, epididymal white AT; FA, fatty acid; FAS, FA synthase; FFA, free FA; FFD, fat-free diet; GSIS, glucose-stimulated insulin secretion; GTT, glucose tolerance test; H&E, hematoxylin and eosin; HFD, high-fat diet; HR, heart rate; HRV, HR variability; HSL, hormone sensitive lipase; iBAC, immortalized brown adipogenic cell; KO, knockout; MG, monoglyceride; NAA, *N*-acetylaspartate; O/N, overnight; OA, oleic acid; PBST, PBS + 0.05% Tween 20; phospho, phosphorylated; PI, phosphatase inhibitor; PIC, protease inhibitor mixture; RER, respiratory exchange ratio; sWAC, subcutaneous white adipogenic cell; sWAT, subcutaneous white AT; TBST, Tris-buffered saline +0.05% Tween 20; TCA, tricarboxylic acid; TG, triglyceride; UCP1, uncoupling protein 1; WT, wild type

[1] Correspondence: Institute of Biochemistry, Graz University of Technology, Humboldtstrasse 46/3, 8010 Graz, Austria. E-mail: juliane.bogner-strauss@tugraz.at

doi: 10.1096/fj.201801323R
This article includes supplemental data. Please visit *http://www.fasebj.org* to obtain this information.

 0892-6638/19/0033-13808

Maintenance of energy homeostasis is a fundamental premise for survival and health of an organism. It requires a balance between mechanisms controlling energy intake—mainly in the form of carbohydrates, lipids, and proteins—and mechanisms of energy expenditure, including basal metabolism, heat production, and physical activity (1). Adipose tissues (ATs) are crucial in these processes. Unilocular white adipocytes can store excessive energy in the form of triglycerides (TGs) in lipid droplets (2) and release stored energy upon energy demand *via* lipolysis, thereby supplying peripheral tissues with fatty acids (FAs) (3–5). Multilocular brown adipocytes are densely packed with mitochondria containing uncoupling protein 1 (UCP1), enabling them to uncouple oxidative phosphorylation from ATP synthesis and generate heat instead (5). ATs are also a sink for circulating glucose, which is mainly used to synthesize lipids *de novo* from glycolysis-derived acetyl–coenzyme A (CoA) (2, 6–10).

Acetyl-CoA *per se* is an important energy metabolite and second messenger (11). Besides glucose, other metabolites, including FA, branched-chain amino acids, or acetate, can be sources for acetyl-CoA (11, 12). Another highly abundant metabolite, namely, *N*-acetylaspartate (NAA), is considered as a storage and transport form of acetyl-CoA in the brain and is primarily used for myelin lipid synthesis (13, 14).

NAA is synthesized by aspartate *N*-acetyltransferase (Asp-NAT; gene: *Nat8l*) from aspartate and acetyl-CoA, and subsequently catabolized by aspartoacylase (ASPA) to acetate and L-aspartate (15–18), building the so-called NAA pathway. Acetyl-CoA synthetase further converts the acetate moiety to acetyl-CoA.

Changes in NAA metabolism are associated with a variety of pathologic conditions. Defective NAA synthesis or catabolism due to mutation of *Nat8l* (hyperacetylaspartia) or *Aspa* (Canavan disease), respectively, lead to severe myelination defects (19–21). Furthermore, NAA levels are reduced in several neuropathologies, such as Alzheimer's disease, ischemic stroke, traumatic brain injury, epilepsy, and multiple sclerosis (22–27), in which NAA is thought to serve as an energy source for the recovery of damaged brain areas (24). Moreover, several aggressive types of cancer, including melanoma, breast, colon, and uterine cancers, show an up-regulation of NAA synthesis. Knockdown of *Nat8l* significantly reduced cancer cell viability, thus suggesting an important role of the NAA pathway in tumor metabolism (28).

Recent publications of our group showed that the NAA pathway is also present in ATs (6, 29, 30), wherein the pathway is regulated by the nutritional state and activated by exogenous glucose—the main source for NAA synthesis in adipocytes (30). Moreover, the NAA pathway was found to regulate lipid turnover, energy metabolism, and histone acetylation in brown adipocytes (6, 29, 30). However, the *in vivo* relevance of this pathway in peripheral tissues remained elusive.

Here we report that NAA is a crucial metabolite for survival on a fat-free diet (FFD) during adolescence. We further show that the NAA pathway is important for modulation of adipocyte lipid turnover and energy balance *in vitro* and *in vivo*. In adult mice, disruption of the NAA pathway in AT leads to an improved metabolic phenotype in mice, as evidenced by increased glucose clearance and energy dissipation. NAA supplementation, in turn, has negative effects on metabolism. Together, our results highlight NAA as an important energy metabolite for the regulation of whole-body energy homeostasis, which needs to be tightly controlled for maintenance of metabolic health.

MATERIALS AND METHODS

Animal studies

All animal procedures followed the *Guide for the Care and Use of Laboratory Animals* (National Institutes of Health, Bethesda, MD, USA), and were approved by the Austrian Ministry of Science, Research, and Economy, and by the local Animal Experimentation Committee of Japan. All experiments were performed in accordance with these guidelines and regulations. Male C57BL/6 mice, *Nat8l*-knockout (KO) mice, first described by Furukawa-Hibi *et al.* (31), and wild-type (WT) littermates were used for this study. Furthermore, AT-specific (ako) *Nat8l*-ko mice were generated by breeding *Nat8l*-floxed mice [a kind gift of M. Eckhardt, Institute of Biochemistry and Molecular Biology, University of Bonn (32)] with mice expressing Cre recombinase under the adiponectin (AdipoQ)-promoter (B6;FVB-Tg(Adipoq-cre)1Evdr/J). Animals were kept on a 14-10 h light/dark cycle and were fed a chow diet (CD; V1126, ssniff Spezialdiäten, Soest, Germany), high-fat diet (HFD; E15744-34.acc. D12451; ssniff Spezialdiäten) or FFD (E15100-04; ssniff Spezialdiäten). Tissues were harvested from mice in fed *ad libitum* or 1-h refed state after being unfed overnight at room temperature and snap frozen in liquid nitrogen.

Bioinformatic analyses

Bioinformatic analyses of *Nat8l* expression in human subcutaneous white adipose tissue (sWAT) (33) and murine sWAT (GN Accession: GN778) was performed using GeneNetwork (*www.genenetwork.org*). Enrichment/pathway analysis was performed using EnrichR (*https://www.ncbi.nlm.nih.gov/pmc/articles/PMC4987924/*) (34, 35).

Murine stromal vascular cell isolation, differentiation, and lipid quantification

sWAT was dissected from C57BL/6, WT, or *Nat8l*-ko mice (CD, 8–12 wk old) and washed in cold DMEM. Tissues were homogenized using a scalpel and digested using a 2 ml/g tissue Collagenase D (0.15 U/ml)/Dispase II (2.4 U/ml) mix (Roche, Basel, Switzerland) in DMEM at 37°C for 30 min. Ten milliliters DMEM containing 10% fetal bovine serum was added to the cell suspensions. Suspensions were filtered through a 100-μm cell strainer and subsequently centrifuged for 10 min at 500 *g*. The pellet was resuspended in Complete medium (DMEM, 10% fetal bovine serum, 50 U/ml penicillin, 50 μg/ml streptomycin, and 2 mM L-glutamine), and cells were seeded to gelatin-coated plates. Medium was changed 24 h later and thereafter every 48 h. Primary subcutaneous white adipogenic cells (sWACs) were differentiated as previously described (36), and 1 μM rosiglitazone was added for the first 3 d of differentiation. Pictures were taken at ×100 magnification. To stimulate lipolysis, cells were incubated with 10 μM isoproterenol for 4 h. Cellular TG content was determined using Infinity Triglyceride Reagent (Thermo Fisher Scientific, Waltham, MA, USA). Free FA (FFA) content

was determined using NEFA-HR(2) Kit (Fujifilm Wako Diagnostics, Mountain View, CA, USA). Values were normalized to total protein content [Pierce Bicinchoninic Acid Assay (BCA) reagent; Thermo Fisher Scientific]. Lipid staining was performed in fixed cells (10% formalin in PBS, 30 min) using Oil Red O (0.25% in 60% isopropyl alcohol stock solution diluted 3:2 with dH_2O) for 45 min.

Protein isolation and Western blot analysis

Differentiated sWACs were harvested for protein analysis in SDS–lysis buffer [50 mm Tris-HCl, pH 6.8, 10% glycerol, 2.5% SDS, 1× protease inhibitor mixture (PIC), 1 mM PMSF] and the lysates were digested with benzonase. For tissue protein isolation, tissues from WT or *Nat8l*-ko mice were homogenized in RIPA buffer [50 mM Tris-HCl (pH 8), 150 mM NaCl, 1% Triton X-100, 0.5% Na-deoxycholate, 0. 1% SDS] + 1× PIC. Samples were left on ice for 20 min and subsequently centrifuged for 15 min at 4°C at maximum speed. The intermediate phase was transferred into a new tube. Protein concentration was determined using the Pierce BCA Protein Assay Kit (Thermo Fisher Scientific). Thirty to sixty micrograms of protein was subjected to a 10% BisTris gel (NuPAGE; Thermo Fisher Scientific), and gels were blotted to nitrocellulose membranes. The following antibodies were used either in Tris-buffered saline +0.05% Tween 20 (TBST) or PBS + 0.05% Tween 20 (PBST): anti–Asp-NAT [1:1000 in 5% bovine serum albumin (BSA)/TBST, kind gift of E. Van Schaftingen, De Duve Institute, Université Catholique de Louvain, Bruxelles, Belgium (15)], anti–phosphorylated (phospho)–acetyl-CoA carboxylase (ACC), anti-ACC and anti–FA synthase (FAS; 1:1000 in 5% BSA/PBST, 8335; Cell Signaling Technology, Danvers, MA, USA), anti-phospho–hormone sensitive lipase (HSL; Ser660) (1:1000 in 5% BSA/TBST, 4126; Cell Signaling Technology), anti-HSL (1:1000 in 5% BSA/TBST, 4107; Cell Signaling Technology,), anti–adipose TG lipase (ATGL; 1:2000 in TBST, 10006409; Cayman Chemicals, Ann Arbor, MI, USA), Total Oxphos Rodent WB Antibody Cocktail (1:500 in 5% milk/TBST, ab110413; Abcam, Cambridge, MA, USA), anti-UCP1 (1:750 in 1% BSA/TBST, ab10983; Abcam), anti–glyceraldehyde 3-phosphate dehydrogenase (1:1000 in 5% milk/PBST, sc-25778; Santa Cruz Biotechnology, Dallas, TX, USA), anti-histone [^{3}H] (1:1000 in 5% BSA/PBST, 44995S; Cell Signaling Technology), anti-hexokinase 1 (1:1000 in 5% BSA/PBST, 2024S; Cell Signaling Technology), anti-acetylated lysine (1:1000 in 5% BSA/PBST, 9681S; Cell Signaling Technology), and anti–β-actin (ACTb; 1:25000 in 1% milk/PBST, A1978; MilliporeSigma, Burlington, MA, USA). For chemiluminescent detection, a horseradish peroxidase–conjugated secondary antibody was used (anti-rabbit 1:2000; anti-mouse 1:3000; Dako, Glostrup, Denmark). Amersham ECL Prime (GE Healthcare, Chicago, IL, USA) or Super Signal West Pico (Thermo Fisher Scientific) served as substrates. ACTb or PonceauS staining served as loading control.

RNA isolation, reverse transcription, and gene expression analysis

Cellular RNA was isolated using the Total RNA Isolation Kit (MilliporeSigma). RNA from tissue was isolated using Trizol reagent (Thermo Fisher Scientific). Reverse transcription for cDNA generation was performed using the QuantiTect Reverse Transcription Kit (Qiagen, Hilden, Germany). Gene expression was assessed using quantitative RT-PCR as previously described (36), and mRNA expression was normalized to TfIIβ. Primer sequences are listed in **Table 1**.

^{14}C-FA uptake

^{14}C-FA uptake of sWACs was performed as previously described (37). Briefly, differentiated sWACs were washed with PBS and preincubated for 1 h with 400 μM oleic acid (OA) containing growth medium. Subsequently, medium was changed to growth medium containing 400 μM OA, 0.1 μCi ^{14}C-OA. After 30 min, cells were washed 3 times with PBS, lysed for 3 h with SDS-NaOH (0.1% SDS/0.3 M NaOH), and radioactivity was measured by liquid scintillation counting.

^{3}H-deoxyglucose uptake of differentiated sWACs

Differentiated sWACs were serum starved for 3 h and then preincubated in DMEM containing 0 g glucose +1 mM sodium pyruvate for 30 min. For the assay, cells were incubated for 30 min in DMEM (25 mM glucose) + 2% BSA + 1 μCi/ml ^{3}H-deoxyglucose. Afterwards, cells were washed 3 times with PBS, lysed for 3 h with SDS-NaOH (0.1% SDS/0.3 M NaOH), and radioactivity was measured by liquid scintillation counting.

^{14}C-glucose incorporation into lipids of differentiated sWACs

^{14}C-glucose incorporation was performed as previously described (37). Differentiated sWACs were incubated for 12 h with growth medium supplemented with 0.1 μCi *D[^{14}C(U)]*- glucose/ml (American Radiolabeled Chemicals, St. Louis, MO, USA).

TABLE 1. *Primer sequences used for quantitative RT-PCR*

Target gene (murine)	Primer sequence, 5′−3′	
	Forward	Reverse
Acc1	TGGTGCAGAGGTACCGAAGTG	CGTAGTGGCCGTTCTGAAACT
Acly	AGGAAGTGCCACCTCCAACAGT	CGCTCATCACAGATGCTGGTCA
Ap2	CGACAGGAAGGTGAAGAGCATC	ACCACCAGCTTGTCACCATCTC
Aspa	CCATATGAAGTGAGAAGGGCTC	CCTCAAGAATAAGAGTGCAACC
Cidea	TGACATTCATGGGATTGCAGAC	GGCCAGTTGTGATGACTAAGAC
Dgat1	GACGGCTACTGGGATCTGA	TCACCACACACCAATTCAGG
Fasn	GCTGTAGCACACATCCTAGGCA	TCGTGTTCTCGTTCCAGGATC
Leptin	GAGACCCCTGTGTCGGTTC	CTGCGTGTGTGAAATGTCATTG
Nat8l	ATCTTCTACGACGGCATCTTGG	GCGGGTCACAGCAAAACAG
Pparγ2	TGCCTATGAGCACTTCACAAGAAAT	CGAAGTTGGTGGGCCAGAA
TfIIβ	GTCACATGTCCGAATCATCCA	TCAATAACTCGGTCCCCTACAA
Ucp1	ACACCTGCCTCTCTCGGAAA	TAGGCTGCCCAATGAACACT

Thereafter, cells were washed 4 times with ice-cold PBS, and neutral lipids were extracted with hexane/isopropanol (3/2, v/v). Thin-layer chromatography was performed with hexane/diethylether/acetic acid (70/29/1, v/v/v) as mobile phase. Lipids were visualized with iodine vapor. Visible bands were cut out, transferred into scintillation cocktail, and incubated overnight. The incorporated radioactivity was measured by liquid scintillation counting in the Tri-Carb 2300TR (Hewlett-Packard, Palo Alto, CA, USA) or the LS6500 (Beckman Coulter, Brea, CA, USA) scintillation counter. Total glucose incorporation into each lipid class was calculated, and values were normalized to protein content.

Cell fractionation of differentiated sWACs

Mitochondrial and cytosolic fractions were isolated freshly from differentiated sWACs (~10×10^6 cells). All steps were performed on ice or at 4°C. Cells were trypsinized, centrifuged at 1200 rpm, and pellets were resuspended in 1 ml HES buffer [20 mM 4-(2-hydroxyethyl)-1-piperazineethanesulfonic acid, 1 mM EDTA, 250 mM sucrose in ddH_2O, pH 7.4] containing 1× PIC mixture and 1× phosphatase inhibitor (PI) mixture (0.1 M Na-orthovanadate, 50 mM Na-glycerophosphate, 0.5 M Na-fluoride). Cell homogenization was performed using a Dounce homogenizer (60 strokes; Thermo Fisher Scientific). Cell debris (500 *g*, 5 min) and nuclei (1000 *g*, 10 min) were removed by centrifugation. The resulting supernatant was centrifuged at 13,000 *g* for 20 min to yield a crude mitochondrial pellet. The pellet was washed 3 times in 1 ml HES buffer containing 1× PIC and 1× PI and was centrifuged again at 13,000 *g* for 20 min. Cell debris (cp), nuclear (nuc), and mitochondrial fraction were resuspended in RIPA buffer + 1× PIC + PI. Cytosolic proteins were precipitated in 100% ice-cold acetone (4/1, v/v) for 2 h at −20°C. Samples were centrifuged at 15,000 *g* for 20 min. Resulting pellet was dried for 10 min at room temperature and resuspended in 150 μl RIPA buffer + 1× PIC + PI.

MitoTracker staining and flow cytometry analysis of differentiated sWACs

Differentiated sWACs from WT and *Nat8l*-ko mice were incubated in Complete growth medium containing 200 nM MitoTracker Red CMXRos (Thermo Fisher Scientific) for 45 min at 37°C. Afterward, cells were washed 3 times with PBS, trypsinized, and centrifuged at 1200 rpm for 5 min, after which the resulting pellet was washed again once with PBS. To exclude dead cells, sWACs were incubated in 200 μl PBS containing 1 μM Sytox blue (Thermo Fisher Scientific) for 15 min at room temperature. Volume was adjusted to 1000 μl with PBS to stop the staining. Cells (1×10^5) were analyzed by flow cytometry using an Attune NxT Flow Cytometer (Thermo Fisher Scientific).

Measurement of cellular and tissue respiration

Differentiated sWACs were plated in Cell-Tak–coated XF96 polystyrene cell culture microplates (Seahorse Bioscience, Billerica, MA, USA) at a density of 20,000 cells per well and were incubated in pH-adjusted culture medium (pH 7.4) containing 0, 1, or 5 mM NAA (MilliporeSigma). After 24 h, cells were washed and preincubated for 30 min in XF assay medium supplemented with sodium pyruvate (1 mM), glutamine (2 mM), and D-glucose (5.5 mM) at 37°C in air. Oxygen consumption rate was subsequently measured every 7 min using an XF96 Extracellular Flux Analyzer (Seahorse Bioscience) and normalized to protein content (pmol O_2/min/mg protein). For measurement of tissue respiration, a Clark electrode (Strathkelvin Instuments, Motherwell, United Kingdom) was used. Freshly isolated tissues from WT and *Nat8l*-ko mice were minced and placed in 100% air-saturated respiration buffer (PBS, 2% BSA, 0.45% D-glucose, 6 mg sodium pyruvate). Oxygen consumption was normalized to tissue weight and calculated as μg O_2/min/mg tissue.

Measurement of cellular and tissue ATP levels

Differentiated sWACs and whole-tissue lysates in RIPA buffer + 1× PIC + 1× PI were used for ATP measurement using CellTiter-Glo Luminescent Cell Viability Assay (Promega, Madison, WI, USA). Samples were diluted with PBS in 96-well plates to a final volume of 100 μl. One hundred microliters of CellTiter-Glo Reagent was added and luminescence read after 5 min incubation at room temperature protected from light.

NAA measurement in tissues

For animal tissues, metabolite extraction was described by Mariño *et al.* (38). Briefly, flash-frozen tissues (60–80 mg) were homogenized using ceramic beads (Circonia beads, N038.1; Carl Roth, Karlsruhe, Germany). Per mg of tissue, 5 μl ice-cold lysis buffer (methanol: water, 80:20, v/v) supplemented with ^{13}C4-*N*-acetylaspartic acid (1 mg/L; MilliporeSigma) were added. Homogenization was performed twice for 20 s at 5500 rpm using the Precellys24 Homogenizer (Bertin Technologies, Montigny-le-Bretonneux, France). Homogenates were centrifuged for 10 min at 12,000 *g* (4°C). Supernatants were lyophilized in a DNA 120 SpeedVac concentrator (ThermoSavant; Bartelt GmbH, Graz, Austria). For analysis, frozen samples were resuspended in analytical-grade water and analyzed *via* HPLC-MS as previously described (29).

Histologic analysis and immunohistochemistry

Tissues were fixed in 4% paraformaldehyde for 24 h and embedded in paraffin. Sections mnesuring 2 μm were cut, deparaffinized using xylene, and stained with hematoxylin and eosin (H&E). Immunohistochemistry was performed using a specific UCP1 antibody (ab10983; Abcam). Antigen retrieval was done using EDTA-sodium buffer (1 mM, pH 8) for 40 min. For incubation and detection, the Dako Real Envision System (K5007; Dako Österreich GmbH, Vienna, Austria) was used. For lipid droplet area and diameter quantification, 100–170 droplets of each genotype were counted.

Measurement of lipolysis from organ explants

Tissues were surgically removed, washed with PBS, and incubated in prewarmed DMEM (4.5 g/L glucose). All further measurements were performed on the same day. Tissue pieces of ~20 mg were preincubated for 1 h in 200 μl DMEM containing 2% FA-free BSA with or without 10 μM isoproterenol at 37°C/5% CO_2/95% humidity atmosphere. After preincubation, fat explants were transferred into 200 μl of identical, fresh medium and incubated for 60 min longer. Medium was collected, and tissue lipids were extracted at 37°C for 1 h using 1 ml chloroform: methanol (2:1, v/v) containing 1% acetic acid. Tissues were lysed overnight in 500 μl NaOH/SDS (0.3 N/0.1%), shaking at 55°C. Protein content was measured using Pierce BCA reagent (Thermo Fisher Scientific). Glycerol release was determined using Infinity Triglyceride Reagent (Thermo Fisher Scientific). FFA release was determined using NEFA-HR (2) Kit (Wako Diagnostics). Values were normalized to protein levels.

Animal phenotyping

All clinical tests were carried out according to the guidelines from the Federation of European Laboratory Animal Science

Associations (Felasa; London, United Kingdom). If not otherwise stated, blood samples were drawn by punctuation of the vena facialis and collected in tubes containing 0.5 M EDTA. Plasma was collected after centrifugation (3600 rpm/10 min/4°C). Glucose was measured with a glucose meter (Calla; Wellion, Marz, Austria) from tail venous blood. Insulin was measured using Mouse Ultrasensitive Insulin ELISA (80-Insmsu-E01; Alpco Diagnostics, Salem, NH, USA). Leptin was measured using a Leptin Mouse ELISA Kit (Crystal Chem, Elk Grove Village, IL, USA). Plasma TG levels were determined using Infinity Triglyceride Reagent (Thermo Fisher Scientific). FFA levels were determined using NEFA-HR kit (2) (Wako Diagnostics). Mice were weighted and food consumption was measured weekly or biweekly. Body temperature was measured using a rectal probe (RET-3; Physitemp Instruments, Clifton, NJ, USA). Life span was monitored from 10 to 36 wk of age.

Glucose and insulin tolerance test

Mice were unfed for 6 h before glucose tolerance test (GTT) and for 4 h for insulin tolerance test. For GTT, mice were injected intraperitoneally with 1.5 g/kg body weight, and for insulin tolerance test with 0.5 U/kg insulin. Glucose was monitored with a glucose meter (Calla; Wellion) from tail venous blood.

Body composition and indirect calorimetric measurements

Body composition was assessed with the miniSpec NMR Analyzer (Bruker Optics, Billerica, MA, USA). For indirect caloric measurements, mice were individually housed in metabolic cages (LabMaster Home Cages System; TSE Systems, Chesterfield, MO, USA; or MK-5000RQ; Muromachi Kikai, Tokyo, Japan) for 2–3 d (20–22°C, 14 h light–10 h dark cycle). Mice were adapted to the metabolic cages for 2 d. Mice were provided with food and water *ad libitum*.

Measurement of *in vivo* lipolysis

Mice were injected in fed state with 1 mg/kg body weight CL-316,243 (CL) compound (C5976; MilliporeSigma). Blood glucose levels were monitored using a glucose meter (Calla; Wellion) from tail venous blood. Blood was collected from vena facialis and plasma FFAs were determined using NEFA-HR (2) Kit (Wako Diagnostics).

In vivo catecholaminergic stress testing

Wt and *Nat8l*-ko mice were lightly anesthetized by isoflurane inhalation (3 and 0.5% for induction and maintenance of anesthesia, respectively), and body temperature was maintained at 37°C using a thermostatically controlled warming pad (TC-1000; CWE, Ardmore, PA, USA). Electrodes were placed subcutaneously in 3 limbs [1-lead electrocardiography (ECG)], and ECG recordings were digitalized and acquired at 2 kHz (Animal Bio Amp, FE136 and MPVS PL3508 PowerLab 8/35; both ADInstruments, Sydney, Australia). After 10-min baseline ECG recording, intraperitoneal injection of adrenalin (Fresenius Kabi, Bad Homburg, Germany) and caffeine (2 mg/kg and 120 mg/kg BW, respectively) was administered to induce catecholaminergic stress and test for any tachyarrhythmias within a 20-min interval.

Heart rate variability analysis

To assess sympathetic activity in mice, heart rate (HR) variability (HRV) analysis was performed. Beat-to-beat alterations in the HR were analyzed offline (LabChart 8 Pro; ADInstruments) using the periodic variation in R-R intervals. ECG signals were scanned for R-wave detection and calculation of R-R intervals and HR. To encompass the progressive bimodal change in HRV (39), 3 stable tracings (baseline, early after injection, peak HR), each of 2-min duration, were studied. Selected segments were examined both visually (on the tachogram) and by automated software functions for the detection of ectopic beats, which were strictly excluded to avoid potential effects on the HRV analysis. All included recordings had <5% of the total beat count identified as ectopic. R-R interval time series were then Hanning-window transformed and studied in the frequency domain (40, 41). For this purpose, we applied the Lomb-Scargle method (HRV module 2, LabChart 8 Pro; ADInstruments), which does not require resampling and replacement of outliers and so can generate robust power spectral density estimates even in the presence of noise or ectopy (42). Low- and high-frequency components of mouse HRV were calculated by integrating the autospectra at the relevant frequency regions (0.4–1.5 Hz and 1.5–4 Hz, respectively). Sympathovagal balance was determined as the low frequency/high frequency ratio.

Glucose-stimulated insulin secretion assay

MIN6 cells were seeded at a density of $2.5 \times 10\text{^}4$ cells/well in 96-well plates in DMEM (4.5 g/L glucose, 61965-026; Thermo Fisher Scientific) containing 15% fetal calf serum. Eighteen hours prior to the experiments, culture medium was switched to low glucose medium (DMEM, 1 g/L glucose, 11966-025; Thermo Fisher Scientific) containing 15% fetal calf serum. Cells were washed once with PBS and preincubated in HBSS (H8262; MilliporeSigma) containing 0.2% protease and FA-free BSA (11945; Serva Electrophoresis GmbH, Heidelberg, Germany) and 2 mM D-glucose (HN06.3; Roth, Newport Beach, CA, USA) for 2 h. Thereafter, insulin secretion was assessed in HBSS supplemented with NAA (00920; MilliporeSigma) and D-glucose as indicated in the figure legends. Supernatants were collected after a 2-h incubation in a humidified incubator. Cells were lysed in RIPA buffer containing PI and PIC. Insulin was measured using the Mouse Ultrasensitive Insulin ELISA (80-INSMSU-E01; Alpco Diagnostics).

Lipid extraction and mass spectrometry

Total lipids from mouse tissues were extracted according to the Folch method (43). Lipid extracts were analyzed by ultra-performance liquid chromatography-quadrupole time of flight-mass spectrometry as previously described (44). In brief, samples were separated using an Aquity Ultra-Performance Liquid Chromatography System (Waters, Milford, MA, USA) equipped with a BEH-C18-column, 2.1×150 mm, 1.7 μm (Waters). The gradient started from 55% solvent A (methanol/water 1/1, v/v) and 45% solvent B (isopropanol), both containing phosphoric acid (8 μM), ammonium acetate (10 mM), and formic acid (0.1 vol%) and reached 100% solvent B within 32 min at a flow rate of 150 μl/min. A Synapt G1 quadrupole time of flight high-definition mass spectrometer (Waters) equipped with an electrospray ionization source was used for analysis in positive and negative ionization mode. Data analysis was performed using the Lipid Data Analyzer software (*http://genome.tugraz.at/lda2/lda_description.shtml*) (45).

Statistical analysis

If not otherwise stated, results are shown as means ± SD with all individual data points of at least 3 independent experiments, or results show 1 representative experiment of 3. Statistical analysis was performed on all available data. Statistical significance was determined using the 2-tailed Student's *t* test, 1-way ANOVA with subsequent Tukey's multiple comparisons test, or 2-way

ANOVA with subsequent Sidak's multiple comparisons test. Significant values were determined when $P < 0.05$.

RESULTS

Central NAA availability is essential on FFD during adolescence

Results from our previous studies (6, 29, 30), together with the *in silico* analysis of published Genotype-Tissue Expression data from human sWAT (33) (**Fig. 1*A***), point to an important role of the NAA pathway in peripheral glucose, lipid, and energy metabolism. To validate these findings *in vivo*, we characterized the metabolic phenotype of WT control and whole-body *Nat8l*-ko mice (Fig. 1*B*, *C*). *Nat8l*-ko mice not only showed significantly reduced NAA levels in the brain but also in brown adipose tissue (BAT) and sWAT (Fig. 1*D*), thus suggesting Asp-NAT as the main NAA biosynthetic enzyme. In line with previous results (32), only 75% of *Nat8l*-ko mice survived until the age of 36 wk when fed either a CD or HFD (Supplemental Fig. S1*A*). Cardiac failure—a common reason for sudden death (46–48)—could be excluded as reason for the reduced survival, as all *Nat8l*-ko mice survived a cardiac stress test (Supplemental Fig. S1*B*–*E*).

To assess the importance of the NAA pathway for whole-body lipid and energy metabolism, we next challenged *Nat8l*-ko mice with a FFD directly after weaning. Although all WT mice survived this treatment, 75% of *Nat8l*-ko mice died (Fig. 1*E*). Notably, supplementation of NAA in drinking water improved the survival of *Nat8l*-ko mice on FFD (Fig. 1*E*). Analysis of tissue NAA levels revealed an increase of brain, BAT, and sWAT NAA levels with NAA supplementation in WT and *Nat8l*-ko mice (Fig. 1*F*). To evaluate whether central NAA deficiency in the brain or peripheral NAA deficiency in AT is responsible for the diminished survival of *Nat8l*-ko mice, we generated *Nat8l*-ako mice by breeding *Nat8l*-floxed mice with mice expressing Cre recombinase under the AdipoQ promotor (Fig. 1*G*, *H* and Supplemental Fig. S1*F*). Even though *Nat8l*-ako mice showed significantly reduced NAA levels in AT (Fig. 1*H*), none of the *Nat8l*-ako mice died throughout the observation period. Moreover, all control and *Nat8l*-ako mice survived the FFD challenge (Supplemental Fig. S1*G*). Together, our data suggest that instead central rather than peripheral NAA availability is important for juvenile survival on FFD.

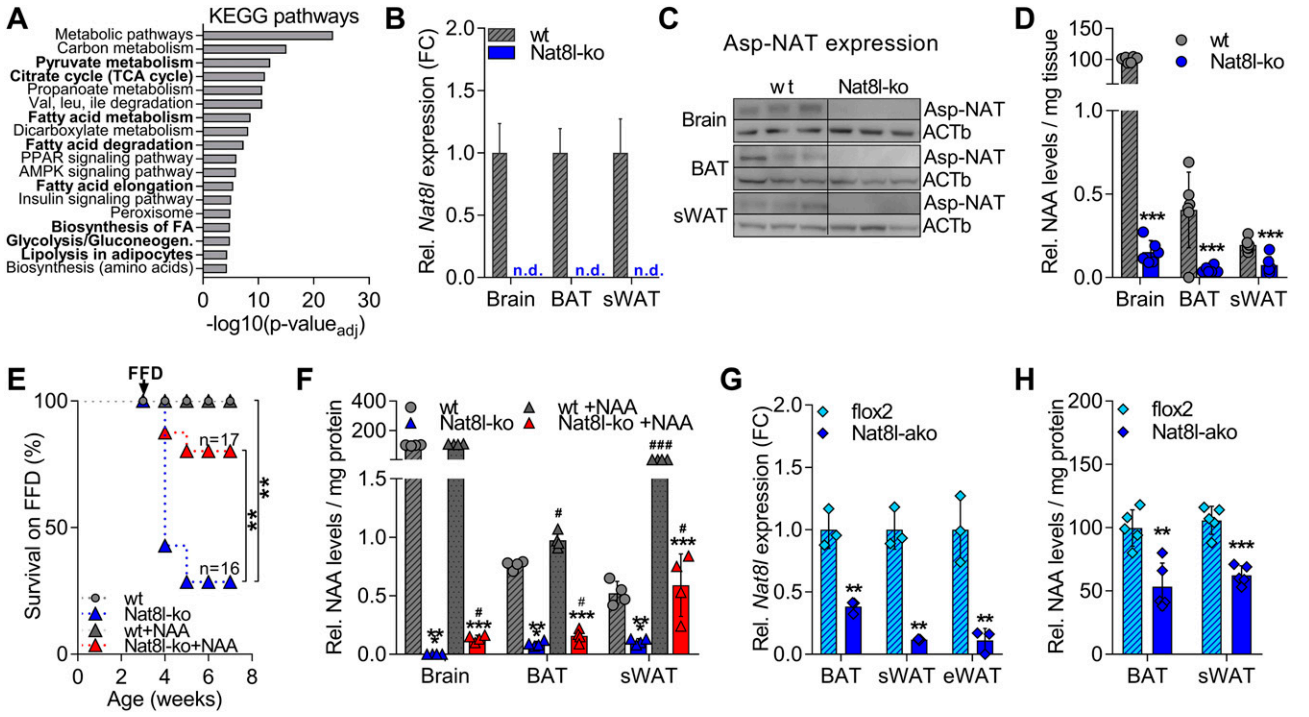

Figure 1. Young *Nat8l*-ko mice depend on dietary fat. *A*) KEGG pathway analysis of the top 1000 genes positively correlated with *Nat8l* expression in human sWAT (33) performed with EnrichR (34, 35). *B*, *C*) Analysis of *Nat8l* mRNA [means ± SD, fold-change (FC) to WT] (*B*) and Asp-NAT protein expression (*C*) in brain, BAT and sWAT in WT and *Nat8l*-ko mice on CD ($n = 3$). *D*) NAA levels in brain, BAT, and sWAT of WT and *Nat8l*-ko mice, ($n = 4$). *E*, *F*) WT and *Nat8l*-ko mice were fed a FFD directly after weaning. NAA (10 mM) was supplemented in drinking water directly after birth. *E*) Survival of WT and *Nat8l*-ko mice on FFD with or without NAA supplementation was monitored until 8 wk of age, [$n = 18$ (WT), $n = 16$ (*Nat8l*-ko), $n = 16$ (WT + NAA), $n = 17$ (*Nat8l*-ko + NAA)]. *F*) NAA levels in brain, BAT and sWAT of WT and *Nat8l*-ko mice with or without NAA supplementation at the age of 8 wk, ($n = 4$). *G*, *H*) *Nat8l*-ako mice were generated by breeding *Nat8l*-floxed mice with mice expressing Cre recombinase under the AdipoQ promotor. Homozygous *Nat8l*-floxed (flox2) mice served as controls. Only male mice on CD were used. *Nat8l* mRNA expression in BAT, sWAT, and eWAT of flox2 and *Nat8l*-ako mice at the age of 22 wk, ($n = 3$) (*G*). NAA levels in BAT and sWAT of flox2 and *Nat8l*-ako mice at the age of 22 wk ($n = 5$) (*H*). N.d., not determined. $^{***}P < 0.001$, $^{****}P < 0.0001$ *vs.* WT (2-tailed Student's t test; *D*, *G*, *H*); $^{**}P < 0.01$ *vs.* WT (log-rank Mantel-Cox test; *E*); $^{***}P < 0.001$ *vs.* control (1-way ANOVA), $^{\#}P < 0.05$, $^{\#\#\#}P < 0.001$ *vs.* untreated (Tukey's multiple comparisons test; *F*).

Nat8l-ko promotes glucose clearance and energy dissipation

To evaluate the relevance of the NAA pathway in AT, we characterized the metabolic consequences of *Nat8l* deficiency. On CD, *Nat8l*-ko mice showed reduced body weight compared with controls throughout life (**Fig. 2*A***). They displayed unchanged body composition (Supplemental Fig. S2*A*) and fat pad weight (Supplemental Fig. S2*B*) but with a trend to reduced epididymal white adipose tissue (eWAT) weight (Supplemental Fig. S2*B*). Furthermore, *Nat8l*-ko mice showed trends to increased energy expenditure (Fig. 2*B*) and physical activity (Supplemental Fig. S2*C*). Despite unchanged plasma leptin levels (Supplemental Fig. S2*D*), cumulative food intake of *Nat8l*-ko mice was increased (Fig. 2*C*). In line with our *in silico* (Fig. 1*A*) and *in vitro* evidence (6, 29, 30), we found that the NAA pathway also affects glucose metabolism *in vivo*. CD-fed *Nat8l*-ko mice showed significantly reduced blood glucose levels in fed and overnight (O/N) unfed states (Fig. 2*D*) despite unchanged respiratory exchange ratio (RER) (Supplemental Fig. S2*E*). Furthermore, glucose tolerance was significantly improved in *Nat8l*-ko mice (Fig. 2*E*). In line, circulating insulin levels after glucose injection were increased by trend in these mice (Fig. 2*F*), yet insulin sensitivity was unchanged (Supplemental Fig. S2*F*). To test, whether *Nat8l*-ko mice also exhibit an improved metabolic phenotype upon diet-induced obesity, we challenged WT and *Nat8l*-ko mice with an HFD. Similar to CD-fed mice, HFD-fed *Nat8l*-ko mice also had reduced body weight throughout life (Fig. 2*G*) and showed overall unchanged body composition (Supplemental Fig. S2*G, H*) with a trend to

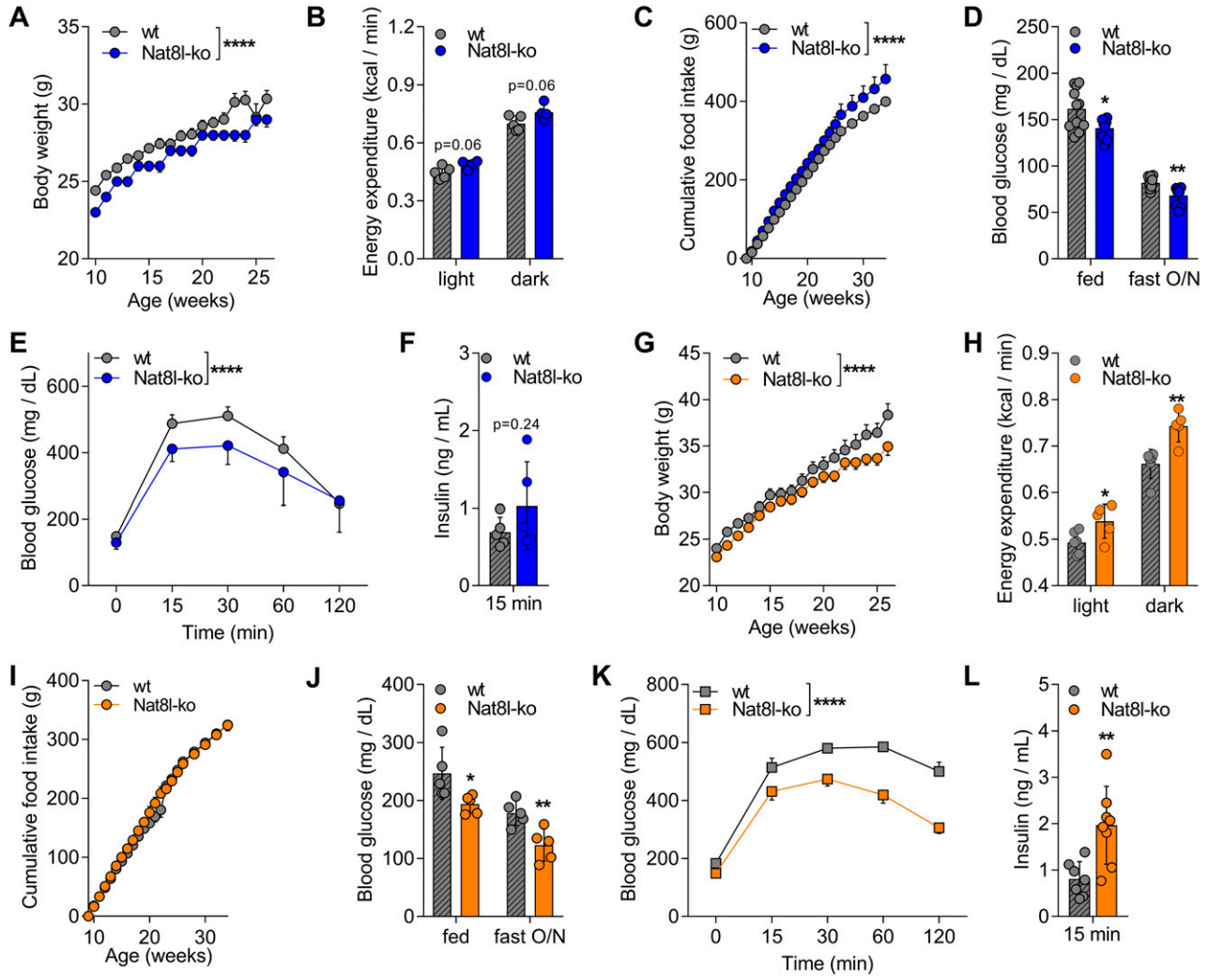

Figure 2. Ko of *Nat8l* reduces body weight and promotes energy dissipation and glucose clearance. *A–F*) Male WT and *Nat8l*-ko mice were fed a CD. Body weight (BW) was monitored until 26 wk of age, ($n = 12/11$) (*A*). Energy expenditure (EE) at the age of 26 wk, ($n = 5/4$) (*B*). Cumulative food intake, ($n = 5$) (*C*). Blood glucose levels in fed and O/N unfed states at the age of 16 wk, ($n = 12/10$) (*D*). Intraperitoneal GTT (ipGTT; 1.5 g glucose/kg BW) at the age of 9 mo, ($n = 10$) (*E*). Plasma insulin levels 15 min after glucose injection (1.5 g glucose/kg BW) at the age of 18 wk, ($n = 5$) (*F*). *G–L*) Male WT and *Nat8l*-ko mice were fed an HFD starting at the age of 8 wk. BW was monitored until 26 wk of age, ($n = 21/17$) (*G*). EE at the age of 26 wk, ($n = 6/5$) (*H*). Cumulative food intake, ($n = 7$) (*I*). Blood glucose levels in fed and O/N unfed state at the age of 16 wk, ($n = 5$) (*J*). IpGTT (1.5 g glucose/kg BW) at the age of 26 wk, ($n = 7/8$) (*K*). Plasma insulin levels 15 min after glucose injection (1.5 g glucose/kg BW) at the age of 22 wk ($n = 7/8$) (*L*). Data are presented as means ± SD. $^*P < 0.05$, $^{**}P < 0.01$ *vs.* WT (2-tailed Student's *t* test), $^{****}P < 0.0001$ *vs.* WT (2-way ANOVA).

reduced sWAT weight (Supplemental Fig. S2*H*). Moreover, HFD-fed *Nat8l*-ko mice showed significantly increased energy expenditure (Fig. 2*H*) despite unchanged physical activity (Supplemental Fig. S2*I*). Cumulative food intake of *Nat8l*-ko mice was unchanged (Fig. 2*I*) and plasma leptin levels were increased (Supplemental Fig. S2*J*). Furthermore, HFD-fed *Nat8l*-ko mice displayed reduced blood glucose levels in fed and O/N unfed states (Fig. 2*J*) together with an increased RER (Supplemental Fig. S2*K*) and improved glucose tolerance (Fig. 2*K*). Notably, *Nat8l*-ko mice also showed elevated plasma insulin levels upon glucose injection (Fig. 2*L*). Moreover, HFD-fed *Nat8l*-ko and control mice reacted comparably to the insulin stimulus during an insulin tolerance test (Supplemental Fig. S2*L*). However, in the later phase of the experiment, plasma glucose levels rose faster in *Nat8l*-ko mice than in control mice (Supplemental Fig. S2*L*). Notably, this improved metabolic phenotype of *Nat8l*-ko mice was also present on FFD (Supplemental Fig. S2*M–Q*), which all *Nat8l*-ko mice survived when the dietary switch to FFD happened at 5 instead of 3 wk of age. Collectively, loss of *Nat8l* promotes a healthy metabolic phenotype with reduced body weight, improved glucose clearance, and increased energy dissipation independent of the dietary status.

Nat8l deficiency leads to browning and increased mitochondrial activity in adipocytes

Our recent publications showed that the NAA pathway impacts the brown adipocyte phenotype (6, 29, 30), which might explain the improved metabolic phenotype of adult *Nat8l*-ko mice. Indeed, we observed enhanced browning of AT depots, as assessed by increased expression of brown adipocyte marker gene *Ucp1* (**Fig. 3*A, B*** and Supplemental Fig. S3*A*), reduced lipid droplet size (Fig. 3*C*, upper panel and Supplemental Fig. S3*B, C*), and increased UCP1 staining (Fig. 3*C*, lower panel) in BAT of *Nat8l*-ko mice. Of note, HFD-fed *Nat8l*-ko mice also showed enhanced BAT browning (Supplemental Fig. S3*D–F*). Likewise, UCP1 expression in sWAT of CD-fed *Nat8l*-ko mice was increased (Fig. 3*D, E* and Supplemental Fig. S3*G*), lipid droplet size reduced (Fig. 3*F*, upper panel and Supplemental Fig. S3*H, I*), and UCP1 staining increased (Fig. 3*F*, lower panel). Accordingly, body temperature of *Nat8l*-ko mice was increased on CD (Fig. 3*G*) yet was unchanged on HFD (Supplemental Fig. S3*J*).

In brown adipocytes, Asp-NAT localizes to mitochondria (6) and ASPA to the cytosol (29). Manipulation of either of the 2 significantly affected mitochondrial number and activity (6, 29). Our bioinformatic analyses suggested that Asp-NAT localizes to mitochondria also in human (Supplemental Fig. S3*K*) and murine (Supplemental Fig. S3*L*) white adipocytes. Indeed, fractionation of differentiated stromal vascular cells (sWACs) isolated from sWAT of C57BL/6 mice confirmed that Asp-NAT localizes to mitochondria in white adipocytes, whereas the NAA catabolizing enzyme ASPA localizes to the cytosol (Supplemental Fig. S3*M*). To investigate the consequences of *Nat8l* deficiency on mitochondrial function, we analyzed differentiated sWACs from WT and *Nat8l*-ko mice, which showed unchanged differentiation capacity (Supplemental Fig. S3*N*). Of note, *Nat8l*-ko cells showed increased MitoTracker signal (Fig. 3*H*), suggesting higher mitochondrial content. We hypothesized that Asp-NAT uses mitochondrial aspartate and acetyl-CoA for NAA synthesis, thereby modulating the tricarboxylic acid (TCA) cycle, cellular respiration, and ATP synthesis. In line with our hypothesis, *Nat8l*-ko sWACs (Fig. 3*I*) as well as BAT and sWAT (Fig. 3*J*) showed higher respiration capacity than controls. Accordingly, ATP levels (Fig. 3*K*) and ATP synthase subunit α (ATP5A-CV) expression (Fig. 3*L*) were also increased in sWACs from *Nat8l*-ko mice, whereas the expression of other mitochondrial respiratory chain complexes was unchanged (Fig. 3*L*). Notably, ATP levels were also increased in *Nat8l*-ko BAT and sWAT (Fig. 3*M*). Similarly, *Nat8l*-ko BAT and sWAT, as well as *Nat8l*-ko sWACs, showed increased *Ucp1* expression (Fig. 3*N*). Together, these results strongly suggest that Asp-NAT and the NAA pathway are involved in regulating energy balance and browning of adipocytes.

ATs mediate the metabolic but not the survival phenotype of *Nat8l*-ko mice

Nat8l deficiency in brain was shown to induce behavioral deficits (49), which might impact AT and whole-body metabolism. To exclude phenotypic effects coming from the brain or other tissues, we also characterized the metabolic phenotype of *Nat8l*-ako mice. Alike *Nat8l*-ko mice, CD-fed *Nat8l*-ako mice showed reduced body weight compared with controls (**Fig. 4*A***) and unchanged body composition (Supplemental Fig. S4*A*). Food consumption was comparable between *Nat8l*-ako and control mice (Supplemental Fig. S4*B*). Furthermore, *Nat8l*-ako mice showed increased energy expenditure, especially during the dark phase (Fig. 4*B*), whereas physical activity of *Nat8l*-ako mice even tends to be reduced (Fig. 4*C*). During the dark phase, RER of *Nat8l*-ako mice was increased (Fig. 4*D*), suggesting increased glucose utilization. Despite unchanged blood glucose levels in the fed *ad libitum* state (Fig. 4*E*), glucose tolerance was improved in *Nat8l*-ako mice (Fig. 4*F*). Furthermore, glucose-stimulated insulin secretion was increased (Fig. 4*G*), yet insulin sensitivity unaffected in *Nat8l*-ako mice (Supplemental Fig. S4*C*). Of note, HFD-fed *Nat8l*-ako mice also showed reduced body weight (Fig. 4*H*), reduced fed *ad libitum* state blood glucose levels (Fig. 4*I*), improved glucose tolerance (Fig. 4*J*), and, by trend, elevated glucose-stimulated plasma insulin levels (Fig. 4*K*). Furthermore, we ruled out that changes in ectopic lipid accumulation are responsible for the improved glucose homeostasis upon *Nat8l* deficiency, as profiles of TGs (Supplemental Fig. S4*D, E*), diglycerides (DGs) (Supplemental Fig. S4*F, G*), ceramides (Supplemental Fig. S4*H, I*), and acylcarnitines (Supplemental Fig. S4*J, K*) in skeletal muscle and liver were comparable between control and *Nat8l*-ako mice, which suggests that the metabolic benefits of *Nat8l* deficiency are indeed mediated by ATs. In line, we observed increased sWAT

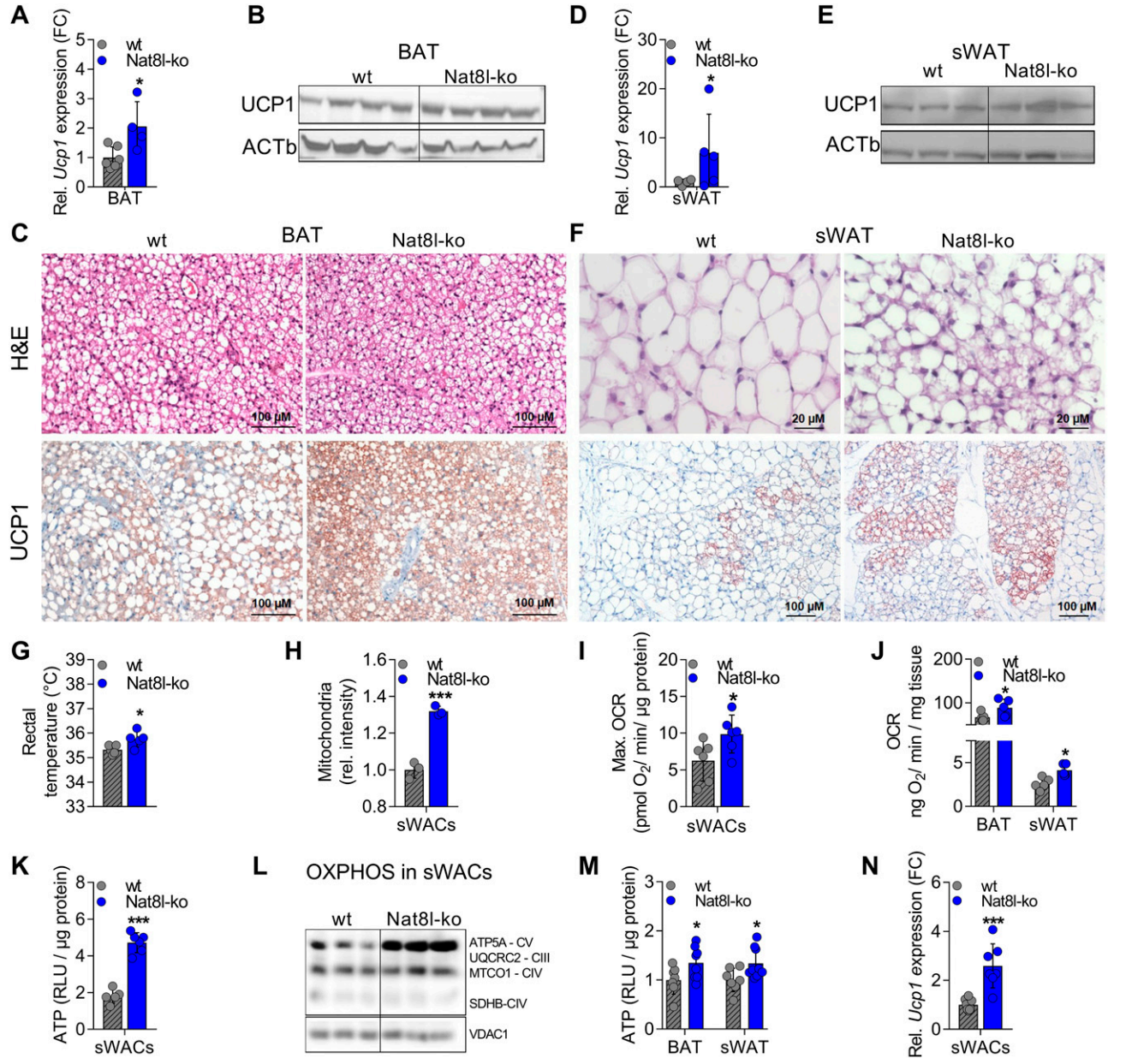

Figure 3. *Nat8l* deficiency leads to browning and increases mitochondrial activity in brown and white adipocytes. Male WT and *Nat8l*-ko mice were fed a CD. *A*) Relative mRNA expression of brown adipocyte marker gene *Ucp1* in BAT from 9-mo-old mice, ($n = 6/4$). *B*) UCP1 protein expression in BAT from 8-wk-old mice. ACTb served as loading control, ($n = 4$). *C*) Representative H&E staining (upper panel) and UCP1 staining (lower panel) of BAT sections from 9-mo-old mice. *D*) Relative *Ucp1* mRNA expression in sWAT of 9-mo-old mice ($n = 5$). *E*) UCP1 protein expression in sWAT from 8-wk-old mice. ACTb served as loading control ($n = 3$). *F*) Representative H&E staining (upper panel) and UCP1 staining (lower panel) of sWAT sections from 9-mo-old mice. *G*) Rectal temperature at the age of 9 mo ($n = 5$). *H*) Stromal vascular cells were isolated from sWAT of WT and *Nat8l*-ko mice and differentiated to adipocytes (sWACs). sWACs were stained with MitoTracker, and fluorescence intensities were determined using flow cytometry ($n = 3$). *I*) Maximal oxygen consumption rate (OCR) of sWACs after stimulation with 0.7-µM FCCP determined using Seahorse Technology ($n = 6$). *J*) Tissue O_2 consumption of BAT and sWAT at age of 9 mo ($n = 5$). *K*) Relative ATP levels in sWACs, ($n = 5/6$). *L*) Western blot with mitochondrial extracts from sWACs using Total Oxphos Rodent WB Antibody Cocktail; Voltage-dependent anion-selective channel 1 (VDAC1) served as loading control ($n = 3$). *M*) Relative ATP levels in BAT and sWAT lysates of 10-wk-old mice in 1-h refed state after being unfed O/N ($n = 7/8$). *N*) Relative *Ucp1* mRNA expression in sWACs ($n = 8/7$). $^*P < 0.05$, $^{***}P < 0.001$ *vs.* WT (2-tailed Student's *t* test).

browning in *Nat8l*-ako mice, as evidenced by increased expression of brown adipocyte marker genes on mRNA (Fig. 4*L*) and protein level (Fig. 4*M, N*) and, by trend, reduced lipid droplet size (Fig. 4*O*). Although BAT morphology was comparable between control and *Nat8l*-ako mice (Supplemental Fig. S4*L*), brown adipocyte marker gene expression was increased (Supplemental Fig. S4*M*). In line, body temperature was also increased by trend in *Nat8l*-ako mice (Fig. 4*P*). Thus, disruption of the NAA pathway in AT circumvents the negative effects of systemic NAA deficiency on survival and improves metabolic health.

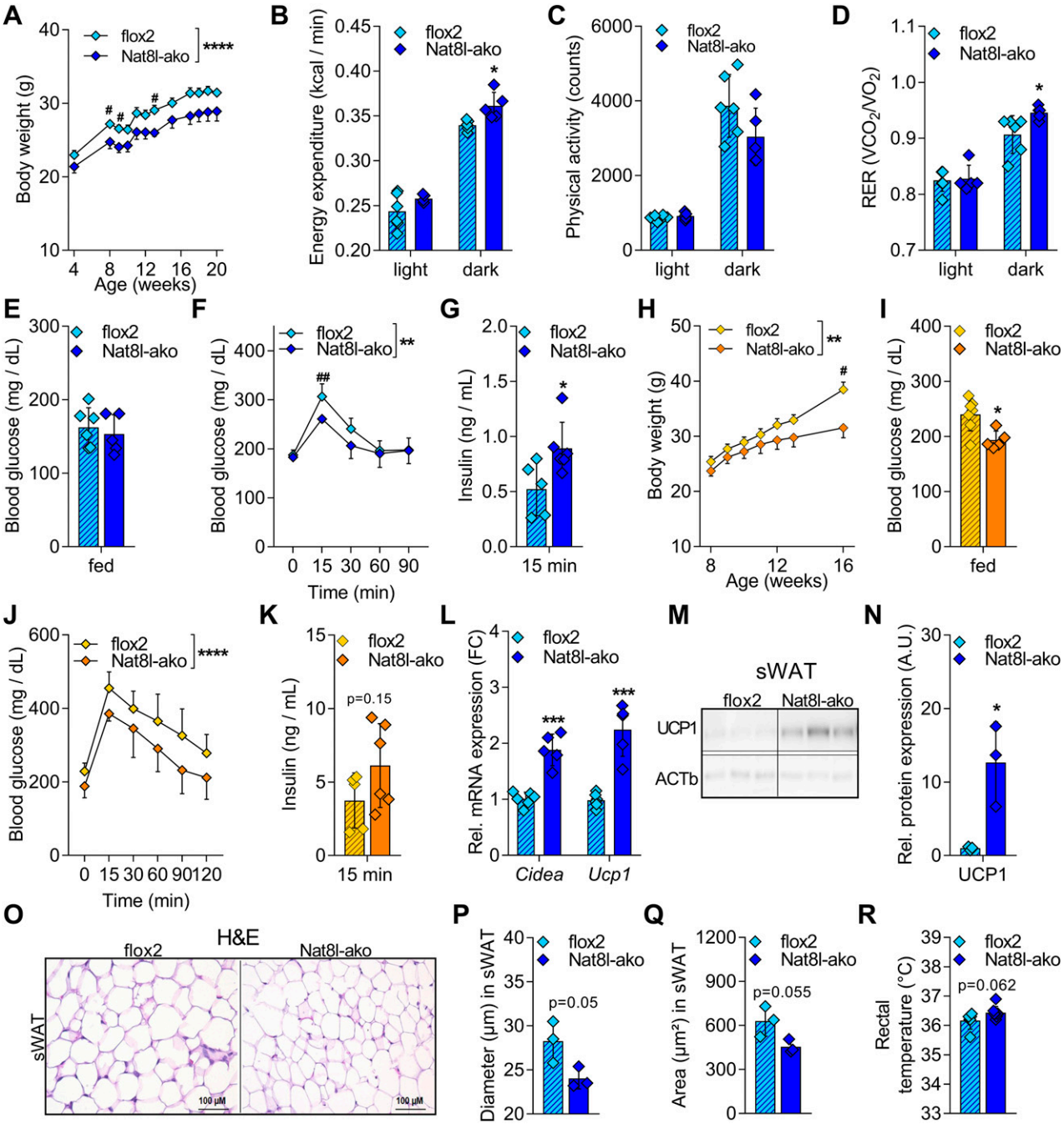

Figure 4. *Nat8l*-ako mice mimic whole-body *Nat8l*-ko mice. Male flox2 and *Nat8l*-ko mice (ako) were fed a CD (*A–G*, *L–R*) or HFD (*H–K*). *A*) Body weight (BW) was monitored until 20 wk of age ($n = 6/5$). *B–D*) Energy expenditure (*B*), physical activity (*C*), and RER (*D*) at the age of 11 wk ($n = 6/5$). *E*) Blood glucose in fed *ad libitum* state at the age of 9 wk ($n = 6/5$). *F*) Intraperitoneal GTT (IpGTT; 1.5 g glucose/kg BW) at the age of 20 wk ($n = 5/6$). *G*) Plasma insulin levels 15 min after glucose injection (1.5 g glucose/kg BW) at the age of 20 wk, ($n = 5/6$). *H*) Body weight was monitored until 16 wk of age ($n = 7/5$). *I*) Blood glucose levels in fed *ad libitum* state at the age of 10 wk ($n = 7/5$). *J*) IpGTT (1.5 g glucose/kg BW) at the age of 16 wk ($n = 7/5$). *K*) Plasma insulin levels 15 min after glucose injection (1.5 g glucose/kg BW) at the age of 16 wk, ($n = 5/6$). *L*) Relative mRNA expression of brown adipocyte marker genes *Cidea* and *Ucp1* in sWAT at the age of 20 wk ($n = 6/5$). *M*) UCP1 expression in sWAT at the age of 20 wk. ACTb served as loading control ($n = 3$). *N*) Quantification of Western blot signal from (*M*) using ImageJ ($n = 3$). *O*) Representative H&E staining of sWAT sections from 20-wk-old mice. *P, Q*) Lipid droplet (LD) diameter (*P*) and area (*Q*) of H&E staining from *O*, showing the mean of >100 LDs per sample ($n = 3$). *R*) Rectal temperature at the age of 18 w, ($n = 6/8$). Data are presented as means ± SD. $^{**}P < 0.01$, $^{****}P < 0.0001$ *vs.* flox2 (2-way ANOVA), $^{\#}P < 0.05$, $^{\#\#}P < 0.01$ *vs.* flox2 (Sidak's multiple comparisons test for individual time points; *A, F, H, J*); $^{*}P < 0.05$, $^{***}P < 0.001$ *vs.* flox2 (2-tailed Student's *t* test; *B–E, G, I, K, L, N, P–R*).

Nat8l deficiency reduces *de novo* lipogenesis and lipolysis in white adipocytes

NAA-derived acetyl-CoA can be used for lipid synthesis in brain (13) and brown adipocytes (6). However, until today, nothing is known about the function of the NAA pathway in white adipocytes. In sWAT of *Nat8l*-ko mice, we found a significant reduction in ACC expression (**Fig. 5*A, B***), which is responsible for the initial step of *de novo* lipogenesis (DNL) from acetyl-CoA. In addition, sWACs isolated from *Nat8l*-ko mice, which showed unchanged adipogenic differentiation (Supplemental Fig. S5*A*), also displayed reduced ACC and FAS expression (Fig. 5*C* and Supplemental Fig. S5*B*), with comparable ratio of phosphorylated (= inactive) to total ACC (Fig. 5*C* and Supplemental Fig. S5*C*). Concomitantly, ^{14}C-glucose incorporation into monoglycerides (MGs), DGs, and TGs was reduced in *Nat8l*-ko sWACs (Fig. 5*D*). However, ^{14}C-glucose incorporation into other lipid classes, such as cholesteryl esters and phospholipids, was unchanged (Fig. 5*D*). Of note, glucose (Supplemental Fig. S5*D*) and FA uptake (Supplemental Fig. S5*E*) was unchanged in these cells.

Besides storage of excessive energy, a main function of adipocytes is to supply peripheral tissues with FAs *via* lipolysis while in an unfed state. In our previous studies, we demonstrated that the NAA pathway potently impacts not only DNL but also lipolysis in brown adipocytes (6, 30). In *Nat8l*-ko sWACs, the expression of key

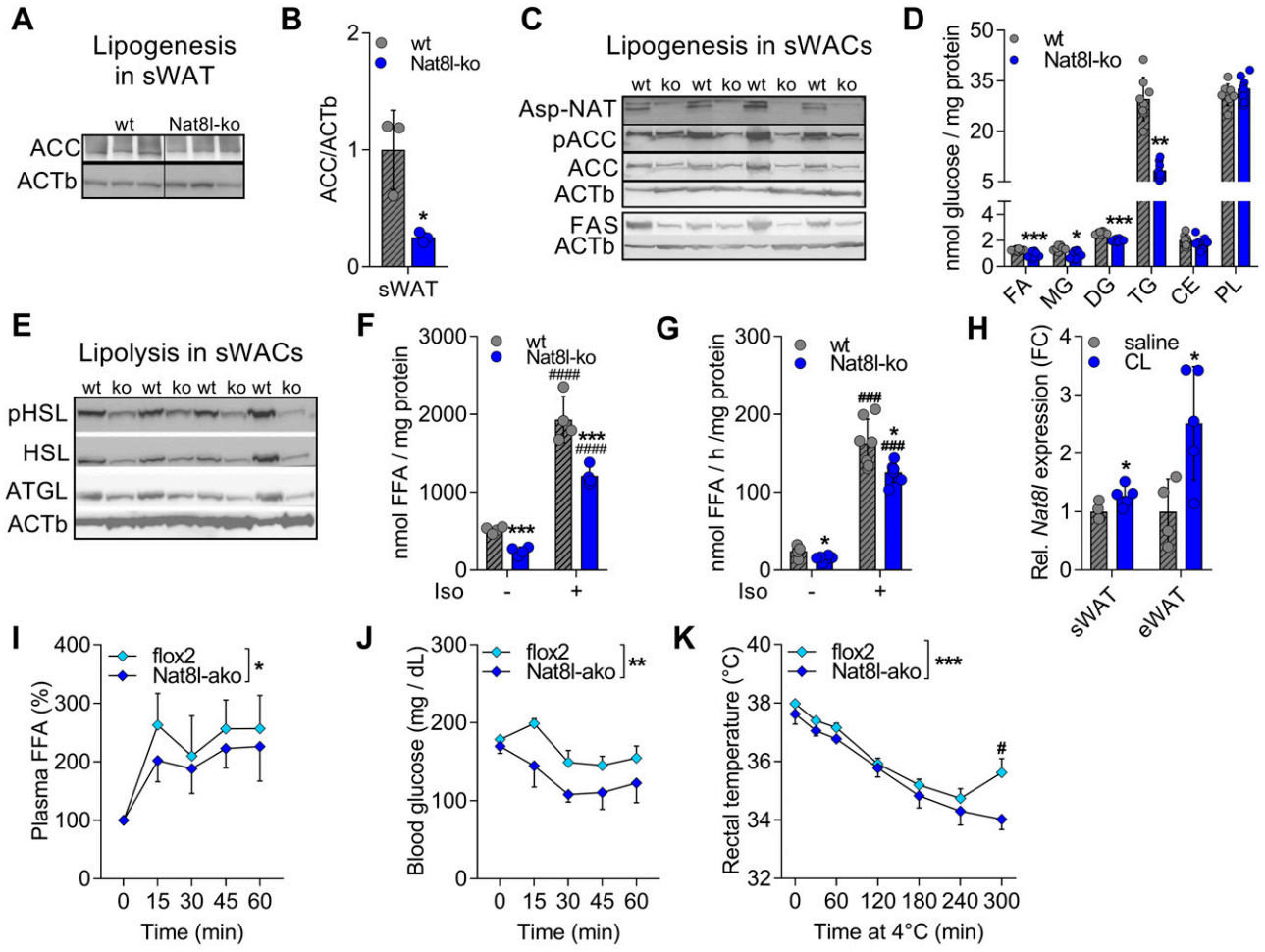

Figure 5. *Nat8l* deficiency impairs lipid turnover in white adipocytes. *A*) Expression of DNL protein ACC in sWAT of 10-wk-old male WT and *Nat8l*-ko mice on CD ($n = 3$). *B*) Quantification of Western blot signal from *A* using ImageJ, ($n = 3$). *C–F*) sWACs from WT and *Nat8l*-ko mice were differentiated to adipocytes for 7 d. *C*) Protein expression of Asp-NAT and DNL-proteins phospho-ACC, ACC, and FAS ($n = 4$). *D*) ^{14}C-glucose incorporation into FAs, MGs, DGs, TGs, cholesteryl esters (CEs), and phospholipids (PLs) ($n = 8$). *E*) Protein expression of key lipases for lipolysis, phospho-HSL, HSL, and ATGL ($n = 4$). *F*) FFA content in the supernatant after 4 h serum starvation with or without isoproterenol treatment (10 μM) ($n = 4$). *G*) FA release from sWAT with or without isoproterenol treatment (10 μM) for 1 h; isolated from 9-mo-old CD-fed male WT and *Nat8l*-ko mice ($n = 7$). *H*) Relative *Nat8l* mRNA expression in sWAT and eWAT from 13-wk-old C57BL/6 mice injected with either 1 mg/kg saline or CL compound for 7 consecutive days ($n = 4/5$). *I, J*) Flox2 and *Nat8l*-ako mice at the age of 10 wk were injected with CL compound (1 mg/kg BW) and plasma FFAs (*I*), and blood glucose levels (*J*) were measured at the indicated time points ($n = 6/5$). *K*) Flox2 and *Nat8l*-ako mice at the age of 15 wk were kept at 4°C without access to food for 5 h. Body temperature was measured at indicated time points ($n = 5/4$). Data are shown as means ± SD. $^{*}P < 0.05$, $^{**}P < 0.01$ *vs.* control (Student's *t* test; *B, D, H*); $^{*}P < 0.05$, $^{***}P < 0.001$ *vs.* WT (1-way ANOVA), $^{\#\#\#}P < 0.001$, $^{\#\#\#\#}P < 0.0001$ *vs.* untreated (Tukey's multiple comparisons test; *F, G*); $^{*}P < 0.05$, $^{**}P < 0.01$, $^{***}P < 0.001$ *vs.* flox2 (2-way ANOVA), $^{\#}P < 0.05$ *vs.* flox2 (Sidak's multiple comparisons test for the individual time points; *I, K*).

lipases for lipolysis, HSL, and ATGL was strongly reduced compared with controls (Fig. 5*E* and Supplemental Fig. S5*F*), with unchanged ratio of phosphorylated (= active) to total HSL (Fig. 5*E* and Supplemental Fig. S5*G*). In line with the reduction of lipase expression, FFA release from *Nat8l*-ko sWACs was also reduced (Fig. 5*F*). Concomitantly, FFA release from sWAT of *Nat8l*-ko mice was reduced (Fig. 5*G*). To test if lipolysis is also impaired *in vivo*, we injected *Nat8l*-ako, *Nat8l*-ko, and respective control mice with CL compound, a strong inducer of lipolysis. Of note, *Nat8l* expression in sWAT and eWAT was increased in C57BL/6 mice when injected with CL compound (Fig. 5*H*). Although CL injection caused a rapid increase in plasma FFA levels in control mice, *Nat8l*-ako (Fig. 5*I*) and *Nat8l*-ko (Supplemental Fig. S5*H*) mice displayed reduced CL-mediated FA mobilization, suggesting that AT lipolysis is impaired upon *Nat8l* deficiency. A drop of blood glucose levels after CL injection confirmed that the treatment worked in all groups (Fig. 5*J* and Supplemental Fig. S5*I*). Moreover, the effect of CL compound on blood glucose levels was much stronger in *Nat8l*-ako and *Nat8l*-ko mice when compared with respective controls (Fig. 5*J* and Supplemental Fig. S5*I*) and is in line with the previous results of improved glucose clearance (Figs. 2*E, K* and 4*F, J*). AT lipolysis was shown to be crucial to maintain body temperature upon acute cold exposure (40). To prove that AT lipolysis is functionally impaired in *Nat8l*-ako mice, we did not feed control and *Nat8l*-ako mice during 5 h of acute cold exposure. Indeed, *Nat8l*-ako mice were not able to maintain their body temperature, whereas controls were able (Fig. 5*K*).

Besides the modulation of lipid synthesis and lipolysis, NAA-derived acetyl-CoA has been implicated in histone and protein acetylation in brown adipocytes (29), a post-transcriptional modification that regulates gene transcription and protein function. Indeed, BAT and sWAT from *Nat8l*-ako mice showed a trend to reduced lysine acetylation within proteins (Supplemental Fig. S5*J, K*), which might contribute to the effects of *Nat8l* deficiency on adipocyte lipid and energy metabolism. Together, our data suggest that the NAA pathway affects lipid turnover and protein acetylation not only in brown but also in white adipocytes.

NAA serves as energy metabolite for lipid synthesis in adipocytes

We hypothesized that NAA serves as energy metabolite that provides acetyl-CoA for lipid synthesis, thereby complementing acetyl-CoA derived from citrate by ATP citrate lyase (*Acly*). To prove this hypothesis, we differentiated sWACs derived from C57BL/6 mice (**Fig. 6*A–F***) and immortalized brown adipogenic cells (iBACs) (Supplemental Fig. S6*A, B*) to white and brown adipocytes, respectively, and treated them with 0, 1, and 5 mM NAA for 24 h. Indeed, NAA treatment increased NAA-catabolizing *Aspa* and reduced *Acly* mRNA expression in these cells (Fig. 6*A* and Supplemental Fig. S6*A*). Notably, expression of white (*Pparγ2*) and brown (*Pgc-1α*) adipocyte differentiation markers were unaffected by the NAA treatment in sWACs (Fig. 6*A*) and iBACs (Supplemental Fig. S6*A*). However, NAA treatment induced lipogenic gene expression (Fig. 6*A, B* and Supplemental Fig. S6*A, C*) and lipid accumulation (Fig. 6*C, D* and Supplemental Fig. S6*B*) in sWACs. Of note, this effect was less pronounced when cells were treated with 5 mM NAA (Fig. 6*B, C* and Supplemental Fig. S6*B*). Furthermore, protein expression of ATGL (Fig. 6*B* and Supplemental Fig. S6*C*) and concomitantly FFA release from sWACs (Fig. 6*E*) was reduced upon NAA treatment, suggesting that NAA serves or signals as energy metabolite. Hence, we measured cellular respiration in sWACs, confirming a dose-dependent decline in cellular respiration upon NAA treatment (Fig. 6*F*). In addition, *Ucp1* expression was also reduced by NAA treatment, both in sWACs (Fig. 6*A*) and iBACs (Supplemental Fig. S6*A*). To assess, whether NAA treatment has similar effects on adipocyte metabolism *in vivo*, we gavaged HFD-fed C57BL/6 mice with either pH-adjusted H_2O or NAA (500 mg/kg body weight) once per week for 19 wk. Like our cell models, NAA-supplemented mice showed increased *Aspa* and reduced *Acly* expression in sWAT (Fig. 6*G*). Furthermore, NAA supplementation increased lipogenic gene expression (Fig. 6*G, H* and Supplemental Fig. S6*D*) and reduced *Ucp1* mRNA (Fig. 6*G*) and protein expression (Fig. 6*I* and Supplemental Fig. S6*E*) in sWAT. Thus, NAA seems to serve as energy metabolite that can be used for lipid synthesis in adipocytes both *in vitro* and *in vivo*.

NAA is an important energy metabolite and crucial during early development

Our data suggested that NAA is crucial in compensating for the reduced dietary fat content during early adolescence (Fig. 1*E*). To prove this hypothesis, we supplemented WT and *Nat8l*-ko mice with NAA (10 mM) in drinking water starting from birth and challenged them with FFD directly after weaning. Of note, NAA supplementation *per se* has previously been shown to have no adverse effects on body weight or food intake in rats (50, 51). On FFD, NAA supplementation not only increased tissue NAA levels and rescued the survival (Fig. 1*E, F*), but the body weight (**Fig. 7*A***) and food intake (Supplemental Fig. S7*A*) were also comparable between WT and *Nat8l*-ko mice. Despite similar body weight, *Nat8l*-ko mice showed improved glucose tolerance (Fig. 7*B*) and trends to increased plasma insulin levels in 1-h refed state (Supplemental Fig. S7*B*) when compared with controls, whereas insulin sensitivity was unaffected (Supplemental Fig. S7*C*). However, glucose levels in fed *ad libitum* and O/N unfed states were unchanged (Supplemental Fig. S7*C*). Other plasma parameters, such as plasma FFA (Fig. 7*C*) and TGs (Fig. 7*D*) were reduced in O/N unfed state. One-hour refeeding did not affect FFA levels (Fig. 7*C*), whereas TG levels remained reduced (Fig. 7*D*). Thus, NAA supplementation seems not to abrogate the effects of *Nat8l* deficiency on glucose and lipid turnover in *Nat8l*-ko mice.

In the following, we were interested in the metabolic consequences of a long-term NAA supplementation in

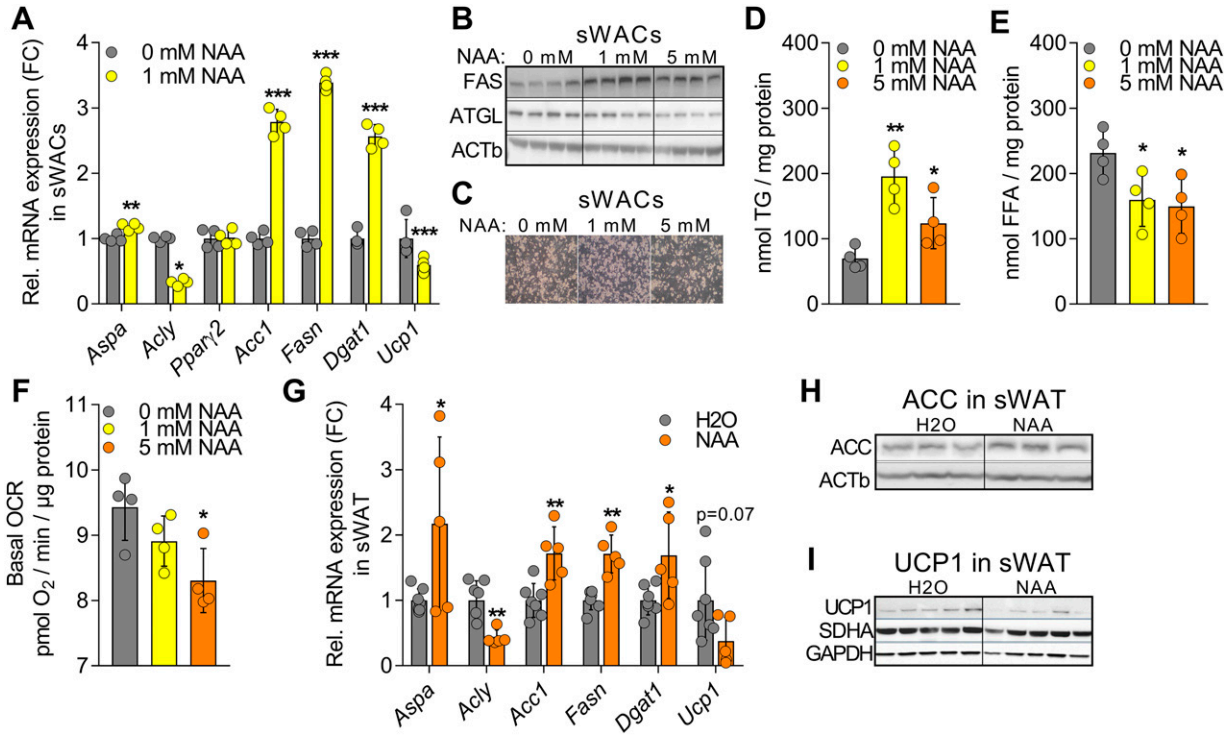

Figure 6. NAA treatment leads to reduced white adipocyte browning and altered lipid turnover. *A–F*) sWACs from C57BL/6 mice were treated from d 6 to 7 of differentiation with indicated concentrations of NAA. Relative mRNA expression of NAA pathway genes (*Aspa*, *Acly*), adipogenesis gene *Pparγ2*, DNL genes (*Acc1*, *Fasn*, *Dgat1*), and brown adipocyte marker gene *Ucp1* ($n = 4$) (*A*). FAS and ATGL protein expression. ACTb served as loading control ($n = 4$) (*B*). Representative images; original magnification, ×100. *D*) Intracellular TG content ($n = 4$) (*C*). FFA content in the supernatant after 4 h of serum starvation ($n = 4$) (*E*). Basal respiration determined by Seahorse Technology ($n = 4$) (*F*). *G–I*) Male C57BL/6 mice were fed an HFD and received either pH-adjusted H_2O or NAA (500 mg/kg BW) once per week *via* oral gavage for 19 wk starting at 6 wk of age. Relative mRNA expression of NAA pathway genes (*Aspa*, *Acly*), DNL genes (*Acc1*, *Fasn*, *Dgat1*), and brown adipocyte marker gene *Ucp1* in sWAT, ($n = 7/5$) (*G*). Protein expression of ACC in sWAT. ACTb served as loading control ($n = 3$) (*H*). Protein expression of UCP1 and mitochondrial oxidative phosphorylation protein succinate dehydrogenase complex flavoprotein subunit A (SDHA) in sWAT (*I*). Glyceraldehyde 3-phosphate dehydrogenase (GAPDH) served as loading control ($n = 5$). $^*P < 0.05$, $^{**}P < 0.01$, $^{***}P < 0.001$ *vs.* control (Student's *t* test).

mice. For this reason, we supplemented HFD-fed C57BL/6 mice with either pH-adjusted H_2O or NAA once per week by oral gavage. Of note, there was no difference between the groups in terms of body weight (Fig. 7*E*), body composition (Supplemental Fig. S7*E*), or food intake (Supplemental Fig. S7*F*), which is in line with previous results of NAA treatment in rats (50). However, NAA treatment decreased energy expenditure (Fig. 7*F*) independent of physical activity (Supplemental Fig. S7*G*). Although glucose levels in fed *ad libitum* and O/N unfed state were unchanged (Supplemental Fig. S7*H*), glucose tolerance of NAA-treated mice was impaired compared with controls (Fig. 7*G*). Furthermore, plasma insulin levels in 1-h refed state after being unfed O/N (Fig. 7*H*) and insulin sensitivity (Fig. 7*I*) were also significantly reduced upon NAA treatment. To address a possible direct effect of NAA on insulin secretion from pancreatic islet cells, we treated MIN6 cells, an established pancreatic β cell line for assessment of glucose-stimulated insulin secretion (GSIS) (52, 53) with different concentrations of NAA. Importantly, NAA treatment significantly reduced GSIS from MIN6 cells when compared with control conditions (Fig. 7*J*). Therefore, changes in pancreatic insulin secretion might—together with the observed changes in AT energy metabolism—contribute to the respective effects of *Nat8l* deficiency and NAA supplementation on glucose metabolism. Taken together, our data provide the first *in vivo* evidence that NAA serves as energy metabolite that impacts adipocyte and whole-body energy homeostasis.

DISCUSSION

In this study we demonstrate a central role of the NAA pathway and the metabolite NAA in regulation of adipocyte and whole-body energy homeostasis.

The NAA pathway is best characterized in the brain, wherein NAA-derived acetyl-CoA is mainly used for myelin lipid synthesis (54). Thus, defects in NAA metabolism by either mutation of *Nat8l*, leading to hypoacetylaspartia, or *Aspa*, leading to Canavan disease, cause severe myelination defects besides other neuropathologies, which in the case of Canavan disease lead to premature death (19–21). As demonstrated by us and others (32), *Nat8l*-ko mice show reduced survival time. The fatality of NAA deficiency became more evident when we challenged *Nat8l*-ko mice with FFD after weaning, seeing as two-thirds of the *Nat8l*-ko mice died. Importantly, NAA

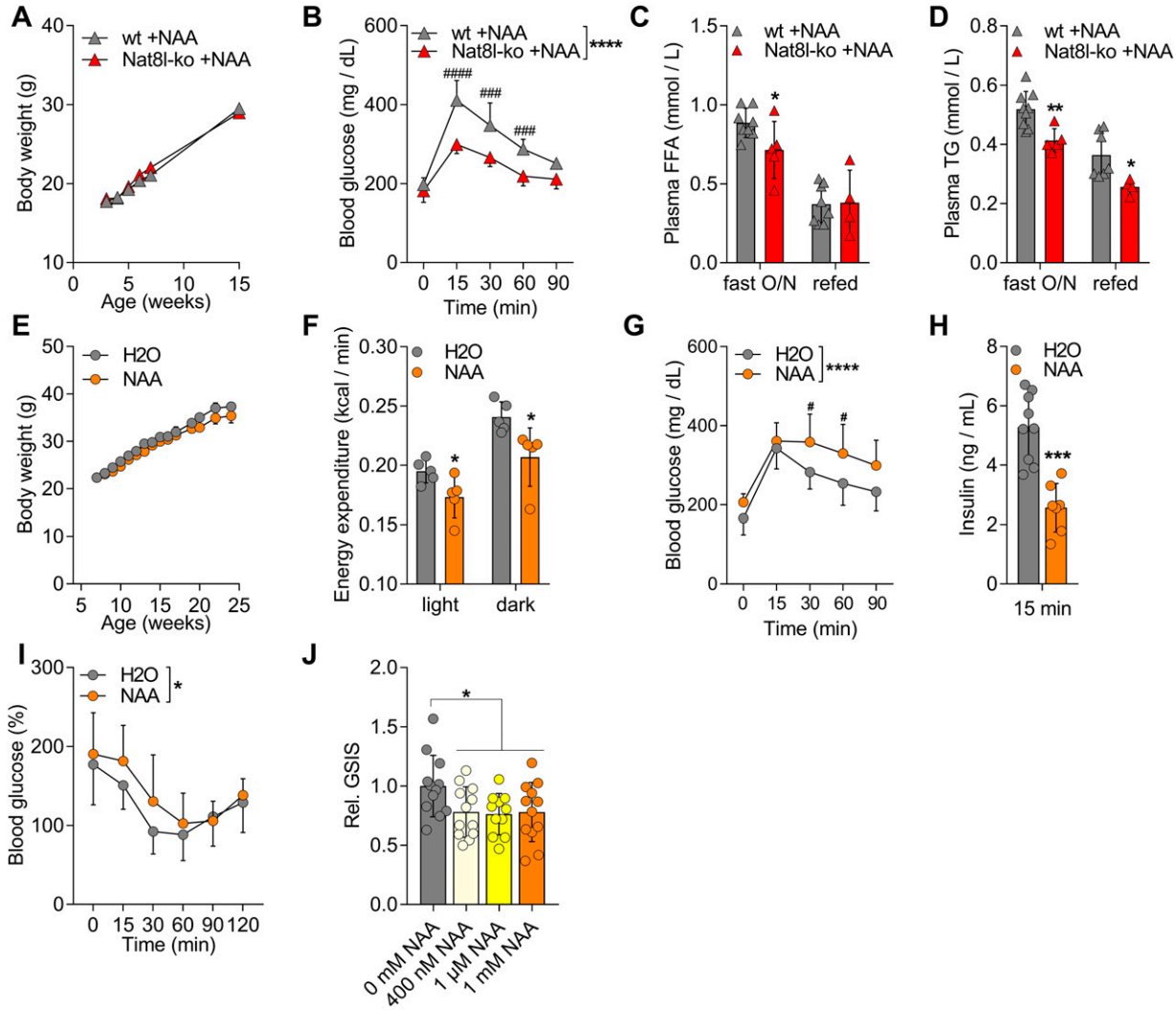

Figure 7. NAA is a powerful energy metabolite that, in excess, impairs metabolic health. *A–D*) WT and *Nat8l*-ko mice were fed with FFD starting at the age of 3 wk. NAA (10 mM) was supplemented in drinking water from birth. Body weight (BW) was monitored until 15 wk of age ($n = 10/9$) (*A*). IpGTT (1.5 g glucose/kg BW) at the age of 9 wk ($n = 7$) (*B*). Plasma FFA (*C*) and TGs (*D*) in O/N unfed ($n = 9/5$) and 1-h refed ($n = 8/4$) states at the age of 8 wk. *E–I*) Male C57BL/6 mice were fed an HFD and received either pH-adjusted H_2O or NAA (500 mg/kg BW) once per week by oral gavage starting at 6 wk of age. BW was monitored until 25 wk of age ($n = 9$) (*E*). Energy expenditure at the age of 23 wk ($n = 5$) (*F*). Intraperitoneal GTT (ipGTT; 1.5 g glucose/kg BW) at 20 wk of age ($n = 9/7$) (*G*). Plasma insulin levels 15 min after glucose injection (1.5 g glucose/kg BW) at 20 wk of age ($n = 9/7$) (*H*). IpITT (0.5 U insulin/kg BW) at 22 wk of age ($n = 9$) (*I*). *J*) GSIS from MIN6 cells during 2-h incubation with HBSS containing 0–1 mM NAA ($n = 12$). Data are shown as means ± SD. $^{*}P < 0.05$, $^{****}P < 0.0001$ *vs.* control (2-way ANOVA); $^{\#}P < 0.05$, $^{\#\#\#}P < 0.001$, $^{\#\#\#\#}P < 0.0001$ *vs.* control (Sidak's multiple comparisons test for individual time points; *A, B, E, G, I*); $^{*}P < 0.05$, $^{**}P < 0.01$, $^{***}P < 0.001$ *vs.* control (2-tailed Student's *t* test; *C, D, F, H, J*).

supplementation from birth significantly increased brain and AT NAA levels and ameliorated the survival on FFD, thus highlighting the relevance for NAA as energy metabolite when dietary lipids are scarce. In line with that, D'Adamo and Yatsu (55) showed that NAA-derived acetate is readily incorporated and preferred over free acetate for lipid synthesis in the brain. Although our data point to the brain as the organ primarily responsible for the high mortality of *Nat8l*-ko mice on FFD, the fact that the reduced body weight of *Nat8l*-ko mice could also be rescued by NAA supplementation suggests a bioenergetic role of NAA beyond the brain. This is supported by results from previous studies that demonstrated that NAA is taken up by peripheral tissues, including the liver, heart, kidney, and mammary gland, where it serves as a source for acetyl-CoA (14, 54, 55). Interestingly, tissues such as the mammary gland preferentially use NAA for lipid synthesis, whereas kidney metabolized NAA very efficiently to CO_2 (18, 55). Although this was known for decades, the relevance of NAA for peripheral metabolism remained elusive.

Although *Aspa* is abundantly expressed in a variety of tissues (29), *Nat8l* is mainly expressed in brain and ATs and hardly detectable in other metabolic tissues (6). Moreover, Asp-NAT is expressed in neurons and ASPA in oligodendrocytes in the brain (54). Thus, NAA has to be shuttled from 1 cell type to another in the brain, whereas brown adipocytes express all enzymes of the NAA pathway (6, 29), indicating a special role of the NAA pathway in ATs. Here, we provide evidence that the whole NAA

pathway is also present in white adipocytes. Furthermore, we found Asp-NAT localized to mitochondria and ASPA in the cytosol in murine white adipocytes. Thus, we hypothesized that the NAA pathway might regulate mitochondrial acetyl-CoA and aspartate availability for the TCA cycle progression. In line, forced overexpression of *Nat8l* in brown adipocytes was shown to drain acetyl-CoA into NAA and activate lipolysis to support cellular respiration (6, 30). Increased cellular respiration and ATP levels in *Nat8l*-deficient adipocytes and ATs further support the idea that surplus acetyl-CoA is used in the TCA cycle when not used for NAA synthesis.

Interestingly, ATs and adipocytes from *Nat8l*-ko mice showed enhanced browning of BAT and sWAT depots. This finding recapitulates our previous data, showing increased mRNA expression of brown marker genes in *Nat8l*-ko BAT and *Nat8l*-silenced brown adipocytes. Back then, increased lipolysis in *Nat8l*-silenced cells, which showed a silencing efficiency of only 50%, was proposed as a possible trigger for browning induction (5, 6, 40). However, *Nat8l*-ko adipocytes and ATs displayed impaired lipolysis. Thus, other mechanisms leading to the browning induction have to be considered. One hypothesis is that the up-regulation of UCP1 represents a compensatory mechanism to get rid of excessive energy that is delivered to the electron transport chain upon *Nat8l* deficiency. Furthermore, MacPherson *et al.* (56) showed that both, pharmacological and genetic lipolysis inhibition in mice can lead to a PKA- mediated increase in UCP1 expression, mitochondrial content, and AT respiration—strongly resembling the phenotype of *Nat8l*-ko mice. Lipolysis is typically activated upon energy demand (57). *Nat8l*-deficient adipocytes showed increased ATP synthesis, which might explain the observed reduction in lipolysis. Furthermore, disruption of the NAA pathway by *Aspa* silencing in brown adipocytes also reduced lipolysis. These cells showed reduced cytosolic acetyl-CoA levels and a global transcriptional repression caused by reduced histone acetylation, which putatively also reduced lipase expression (29). Interestingly, overall protein acetylation and lipase expression were also reduced in *Nat8l*-deficient adipocytes; hence, a similar scenario as observed upon *Aspa* silencing could therefore also be envisioned upon ko of *Nat8l* in adipocytes. Moreover, NAA-treated brown adipocytes showed reduced cellular respiration and lipolysis (29), similar to what we observed in NAA-treated white adipocytes. Thus, NAA *per se*, or NAA-derived acetyl-CoA might signal as energy metabolite, thereby repressing other energy-providing pathways, such as lipolysis and cellular respiration. More focused studies are, however, needed to elucidate a possible crosstalk of the NAA pathway with lipases, PKA, or other metabolic regulators in the future.

We previously suggested that the NAA pathway is an alternative route to citrate and *Acly* to provide cytosolic acetyl-CoA for lipid synthesis in brown adipocytes (6). Disruption of this pathway would therefore reduce cytosolic acetyl-CoA levels and lipid synthesis. This is supported by reduced expression of ACC and/or FAS in AT and adipocytes from *Nat8l*-ko mice. Furthermore, we found reduced glucose incorporation into FAs, MGs, DGs, and TGs in adipocytes from *Nat8l*-ko mice. On the contrary, NAA-treated adipocytes showed increased lipogenic protein expression and lipid accumulation, confirming that the NAA pathway is important for lipid synthesis in white adipocytes and also supports that depletion of NAA leads to a catabolic rather than an anabolic phenotype. Although we propose that the NAA pathway primarily regulates adipocyte metabolism *via* modulation of the subcellular distribution of acetyl-CoA, it should also be considered that NAA, besides acetyl-CoA, carries aspartate and nitrogen from mitochondria to the cytosol. Recent data from Huber *et al.* (30) point to a role of NAA in aspartate metabolism, as knockdown of *Nat8l* in brown adipocytes leads to a strong reduction in intracellular aspartate levels. To date, the fate of (NAA-derived) aspartate has not been investigated but might be used, for example, for protein synthesis or could re-enter the mitochondrial TCA cycle in the form of oxaloacetate for energy production. Thus, the function of the NAA pathway as a shuttle for aspartate or as a nitrogen-acceptor should be addressed in future studies.

Notably, several metabolites, such as glucose and FFA, are known to trigger insulin secretion, whereas others, such as the α-amino acid homocysteine, seem to inhibit insulin secretion (58). Recently, a strong association of 5 aa, including aspartate, with decreases in insulin secretion, elevation of blood glucose levels, and increased risk of type 2 diabetes, was found in humans (59). In line with this, we found that *Nat8l*-ko and *Nat8l*-ako mice showed reduced GSIS. NAA treatment, in contrast, reduced GSIS *in vitro* and *in vivo*. Hence, NAA or NAA-derived acetyl-CoA or aspartate might affect glucose metabolism *via* modulation of pancreatic insulin secretion.

Importantly, we could show that the NAA pathway in ATs has significant impact on whole-body lipid, glucose, and energy homeostasis. Although NAA seems to be crucial during early development, especially under low-fat conditions, NAA deficiency promotes a rather beneficial metabolic phenotype later in life. Both whole-body and *Nat8l*-ako mice showed reduced body weight, increased energy expenditure, and improved glucose clearance. Contrarily, weekly doses of NAA had adverse effects on metabolic health, as NAA-treated mice showed reduced energy expenditure and impaired glucose tolerance and insulin sensitivity.

In summary, our work has demonstrated that the NAA pathway is potent in regulating adipocyte metabolism, and reveals NAA as a powerful metabolite that can—when tightly regulated—determine metabolic health. Given the observation that several cancers show an up-regulation of NAA synthesis (28), targeting the NAA pathway in adult life might represent a promising strategy to combat a broad spectrum of devastating diseases. FJ

ACKNOWLEDGMENTS

The authors thank Thomas Schreiner and Wolfgang Krispel (both from the Institute of Biochemistry, Graz University of Technology) for excellent technical assistance. This work was supported by the Austrian Science Fund (FWF; Grants DK-MCD W1226, P24143, P27108, and P27070). The authors gratefully acknowledge support from Joint Teaching, Research and Doctoral Programmes in the Natural Sciences (NAWI)

Graz and BioTechMed–Graz. The authors declare no conflicts of interest.

AUTHOR CONTRIBUTIONS

D. C. Hofer, G. Zirkovits, H. J. Pelzmann, and J. G. Bogner-Strauss designed the experiments; D. C. Hofer, G. Zirkovits, H. J. Pelzmann, K. Huber, A. R. Pessentheiner, W. Xia, K. Uno, T. Miyazaki, K. Kon, H. Tsuneki, T. Pendl, W. Al Zoughbi, C. T. Madreiter-Sokolowski, G. Trausinger, M. Abdellatif, G. Schoiswohl, and R. Schreiber performed the experiments together with the support of T. Eisenberg, C. Magnes, S. Sedej, M. Eckhardt, M. Sasahara, T. Sasaoka, A. Nitta, G. Hoefler, W. F. Graier, D. Kratky, J. Auwerx, and J. G. Bogner-Strauss; D. C. Hofer, G. Zirkovits, and J. G. Bogner-Strauss wrote the manuscript; and all authors reviewed the final manuscript.

REFERENCES

1. Waterson, M. J., and Horvath, T. L. (2015) Neuronal regulation of energy homeostasis: beyond the hypothalamus and feeding. *Cell Metab.* **22**, 962–970
2. Rosen, E. D., and Spiegelman, B. M. (2014) What we talk about when we talk about fat. *Cell* **156**, 20–44
3. Haemmerle, G., Zimmermann, R., Strauss, J. G., Kratky, D., Riederer, M., Knipping, G., and Zechner, R. (2002) Hormone-sensitive lipase deficiency in mice changes the plasma lipid profile by affecting the tissue-specific expression pattern of lipoprotein lipase in adipose tissue and muscle. *J. Biol. Chem.* **277**, 12946–12952
4. Zimmermann, R., Strauss, J. G., Haemmerle, G., Schoiswohl, G., Birner-Gruenberger, R., Riederer, M., Lass, A., Neuberger, G., Eisenhaber, F., Hermetter, A., and Zechner, R. (2004) Fat mobilization in adipose tissue is promoted by adipose triglyceride lipase. *Science* **306**, 1383–1386
5. Cannon, B., and Nedergaard, J. (2004) Brown adipose tissue: function and physiological significance. *Physiol. Rev.* **84**, 277–359
6. Pessentheiner, A. R., Pelzmann, H. J., Walenta, E., Schweiger, M., Groschner, L. N., Graier, W. F., Kolb, D., Uno, K., Miyazaki, T., Nitta, A., Rieder, D., Prokesch, A., and Bogner-Strauss, J. G. (2013) NAT8L (N-acetyltransferase 8-like) accelerates lipid turnover and increases energy expenditure in Brown adipocytes. *J. Biol. Chem.* **288**, 36040–36051
7. Herman, M. A., Peroni, O. D., Villoria, J., Schön, M. R., Abumrad, N. A., Blüher, M., Klein, S., and Kahn, B. B. (2012) A novel ChREBP isoform in adipose tissue regulates systemic glucose metabolism. *Nature* **484**, 333–338
8. Ma, S. W., and Foster, D. O. (1986) Uptake of glucose and release of fatty acids and glycerol by rat brown adipose tissue *in vivo*. *Can. J. Physiol. Pharmacol.* **64**, 609–614
9. Winegrad, A. I., Shaw, W. N., Lukens, F. D. W., and Stadie, W. C. (1960) Lipogenesis in adipose tissue. *Am. J. Clin. Nutr.* **8**, 651–665
10. Bartelt, A., Bruns, O. T., Reimer, R., Hohenberg, H., Ittrich, H., Peldschus, K., Kaul, M. G., Tromsdorf, U. I., Weller, H., Waurisch, C., Eychmüller, A., Gordts, P. L. S. M., Rinninger, F., Bruegelmann, K., Freund, B., Nielsen, P., Merkel, M., and Heeren, J. (2011) Brown adipose tissue activity controls triglyceride clearance. *Nat. Med.* **17**, 200–205
11. Pietrocola, F., Galluzzi, L., Bravo-San Pedro, J. M., Madeo, F., and Kroemer, G. (2015) Acetyl coenzyme a: a central metabolite and second messenger. *Cell Metab.* **21**, 805–821
12. Gao, X., Lin, S.-H., Ren, F., Li, J.-T., Chen, J.-J., Yao, C.-B., Yang, H.-B., Jiang, S.-X., Yan, G.-Q., Wang, D., Wang, Y., Liu, Y., Cai, Z., Xu, Y.-Y., Chen, J., Yu, W., Yang, P.-Y., and Lei, Q.-Y. (2016) Acetate functions as an epigenetic metabolite to promote lipid synthesis under hypoxia. *Nat. Commun.* **7**, 11960
13. Chakraborty, G., Mekala, P., Yahya, D., Wu, G., and Ledeen, R. W. (2001) Intraneuronal N-acetylaspartate supplies acetyl groups for myelin lipid synthesis: evidence for myelin-associated aspartoacylase. *J. Neurochem.* **78**, 736–745
14. Mehta, V., and Namboodiri, M. A. (1995) N-acetylaspartate as an acetyl source in the nervous system. *Brain Res. Mol. Brain Res.* **31**, 151–157
15. Wiame, E., Tyteca, D., Pierrot, N., Collard, F., Amyere, M., Noel, G., Desmedt, J., Nassogne, M.-C., Vikkula, M., Octave, J.-N., Vincent, M.-F., Courtoy, P. J., Boltshauser, E., and van Schaftingen, E. (2009) Molecular identification of aspartate N-acetyltransferase and its mutation in hypoacetylaspartia. *Biochem. J.* **425**, 127–136
16. Ariyannur, P. S., Moffett, J. R., Manickam, P., Pattabiraman, N., Arun, P., Nitta, A., Nabeshima, T., Madhavarao, C. N., and Namboodiri, A. M. A. (2010) Methamphetamine-induced neuronal protein NAT8L is the NAA biosynthetic enzyme: implications for specialized acetyl coenzyme A metabolism in the CNS. *Brain Res.* **1335**, 1–13
17. Kaul, R., Casanova, J., Johnson, A. B., Tang, P., and Matalon, R. (1991) Purification, characterization, and localization of aspartoacylase from bovine brain. *J. Neurochem.* **56**, 129–135
18. Bogner-Strauss, J. G. (2017) N-acetylaspartate metabolism outside the brain: lipogenesis, histone acetylation, and cancer. *Front. Endocrinol. (Lausanne)* **8**, 240
19. Matalon, R., Michals, K., Sebesta, D., Deanching, M., Gashkoff, P., Casanova, J., Optiz, J. M., and Reynolds, J. F. (1988) Aspartoacylase deficiency and N-acetylaspartic aciduria in patients with canavan disease. *Am. J. Med. Genet.* **29**, 463–471
20. Boltshauser, E., Schmitt, B., Wevers, R. A., Engelke, U., Burlina, A. B., and Burlina, A. P. (2004) Follow-up of a child with hypoacetylaspartia. *Neuropediatrics* **35**, 255–258
21. Burlina, A. P., Schmitt, B., Engelke, U., Wevers, R. A., Burlina, A. B., and Boltshauser, E. (2006) Hypoacetylaspartia: clinical and biochemical follow-up of a patient. In *N-acetylaspartate* (Moffett, J. R., Tieman, S. B., Weinberger, D. R., Coyle, J. T., and Namboodiri, A. M. A., eds.), pp. 283–287, Springer, Boston
22. Larsson, H. B., Christiansen, P., Jensen, M., Frederiksen, J., Heltberg, A., Olesen, J., and Henriksen, O. (1991) Localized *in vivo* proton spectroscopy in the brain of patients with multiple sclerosis. *Magn. Reson. Med.* **22**, 23–31
23. Peeling, J., and Sutherland, G. (1993) 1H magnetic resonance spectroscopy of extracts of human epileptic neocortex and hippocampus. *Neurology* **43**, 589–594
24. Moffett, J. R., Arun, P., Ariyannur, P. S., and Namboodiri, A. M. A. (2013) N-Acetylaspartate reductions in brain injury: impact on post-injury neuroenergetics, lipid synthesis, and protein acetylation. *Front. Neuroenergetics* **5**, 11
25. Signoretti, S., Marmarou, A., Tavazzi, B., Lazzarino, G., Beaumont, A., and Vagnozzi, R. (2001) N-Acetylaspartate reduction as a measure of injury severity and mitochondrial dysfunction following diffuse traumatic brain injury. *J. Neurotrauma* **18**, 977–991
26. Fenstermacher, M. J., and Narayana, P. A. (1990) Serial proton magnetic resonance spectroscopy of ischemic brain injury in humans. *Invest. Radiol.* **25**, 1034–1039
27. Klunk, W. E., Panchalingam, K., Moossy, J., McClure, R. J., and Pettegrew, J. W. (1992) N-acetyl-L-aspartate and other amino acid metabolites in Alzheimer's disease brain: a preliminary proton nuclear magnetic resonance study. *Neurology* **42**, 1578–1585
28. Zand, B., Previs, R. A., Zacharias, N. M., Rupaimoole, R., Mitamura, T., Nagaraja, A. S., Guindani, M., Dalton, H. J., Yang, L., Baddour, J., Achreja, A., Hu, W., Pecot, C. V., Ivan, C., Wu, S. Y., McCullough, C. R., Gharpure, K. M., Shoshan, E., Pradeep, S., Mangala, L. S., Rodriguez-Aguayo, C., Wang, Y., Nick, A. M., Davies, M. A., Armaiz-Pena, G., Liu, J., Lutgendorf, S. K., Baggerly, K. A., Eli, M. B., Lopez-Berestein, G., Nagrath, D., Bhattacharya, P. K., and Sood, A. K. (2016) Role of increased n-acetylaspartate levels in cancer. *J. Natl. Cancer Inst.* **108**, djv426
29. Prokesch, A., Pelzmann, H. J., Pessentheiner, A. R., Huber, K., Madreiter-Sokolowski, C. T., Drougard, A., Schittmayer, M., Kolb, D., Magnes, C., Trausinger, G., Graier, W. F., Birner-Gruenberger, R., Pospisilik, J. A., and Bogner-Strauss, J. G. (2016) N-acetylaspartate catabolism determines cytosolic acetyl-CoA levels and histone acetylation in brown adipocytes. *Sci. Rep.* **6**, 23723
30. Huber, K., Hofer, D. C., Trefely, S., Pelzmann, H. J., Madreiter-Sokolowski, C., Duta-Mare, M., Schlager, S., Trausinger, G., Stryeck, S., Graier, W. F., Kolb, D., Magnes, C., Snyder, N. W., Prokesch, A., Kratky, D., Madl, T., Wellen, K. E., and Bogner-Strauss, J. G. (2019) N-acetylaspartate pathway is nutrient responsive and coordinates lipid and energy metabolism in brown adipocytes. *Biochim. Biophys. Acta Mol. Cell Res.* **1866**, 337–348
31. Furukawa-Hibi, Y., Nitta, A., Fukumitsu, H., Somiya, H., Toriumi, K., Furukawa, S., Nabeshima, T., and Yamada, K. (2012) Absence of SHATI/Nat8l reduces social interaction in mice. *Neurosci. Lett.* **526**, 79–84
32. Maier, H., Wang-Eckhardt, L., Hartmann, D., Gieselmann, V., and Eckhardt, M. (2015) N-acetylaspartate synthase deficiency corrects

the myelin phenotype in a canavan disease mouse model but does not affect survival time. *J. Neurosci.* **35**, 14501–14516
33. GTEx Consortium (2013) The genotype-tissue expression (GTEx) project. *Nat. Genet.* **45**, 580–585
34. Chen, E. Y., Tan, C. M., Kou, Y., Duan, Q., Wang, Z., Meirelles, G. V., Clark, N. R., and Ma'ayan, A. (2013) Enrichr: interactive and collaborative HTML5 gene list enrichment analysis tool. *BMC Bioinformatics* **14**, 128
35. Kuleshov, M. V., Jones, M. R., Rouillard, A. D., Fernandez, N. F., Duan, Q., Wang, Z., Koplev, S., Jenkins, S. L., Jagodnik, K. M., Lachmann, A., McDermott, M. G., Monteiro, C. D., Gundersen, G. W., and Ma'ayan, A. (2016) Enrichr: a comprehensive gene set enrichment analysis web server 2016 update. *Nucleic Acids Res.* **44**(W1), W90–W97
36. Bogner-Strauss, J. G., Prokesch, A., Sanchez-Cabo, F., Rieder, D., Hackl, H., Duszka, K., Krogsdam, A., Camillo, B. D., Walenta, E., Klatzer, A., Lass, A., Pinent, M., Wong, W.-C., Eisenhaber, F., and Trajanoski, Z. (2010) Reconstruction of gene association network reveals a transmembrane protein required for adipogenesis and targeted by PPARγ. *Cell. Mol. Life Sci.* **67**, 4049–4064
37. Hofer, D. C., Pessentheiner, A. R., Pelzmann, H. J., Schlager, S., Madreiter-Sokolowski, C. T., Kolb, D., Eichmann, T. O., Rechberger, G., Bilban, M., Graier, W. F., Kratky, D., and Bogner-Strauss, J. G. (2017) Critical role of the peroxisomal protein PEX16 in white adipocyte development and lipid homeostasis. *Biochim. Biophys. Acta Mol. Cell Biol. Lipids* **1862**, 358–368
38. Mariño, G., Pietrocola, F., Eisenberg, T., Kong, Y., Malik, S. A., Andryushkova, A., Schroeder, S., Pendl, T., Harger, A., Niso-Santano, M., Zamzami, N., Scoazec, M., Durand, S., Enot, D. P., Fernández, Á. F., Martins, I., Kepp, O., Senovilla, L., Bauvy, C., Morselli, E., Vacchelli, E., Bennetzen, M., Magnes, C., Sinner, F., Pieber, T., López-Otín, C., Maiuri, M. C., Codogno, P., Andersen, J. S., Hill, J. A., Madeo, F., and Kroemer, G. (2014) Regulation of autophagy by cytosolic acetyl-coenzyme A. *Mol. Cell* **53**, 710–725
39. Leor-Librach, R. J., Eliash, S., Kaplinsky, E., and Bobrovsky, B.-Z. (2003) Very low-frequency heart rate variability wave amplitude and sympathetic stimulation–characterization and modeling. *IEEE Trans. Biomed. Eng.* **50**, 797–803
40. Schreiber, R., Diwoky, C., Schoiswohl, G., Feiler, U., Wongsiriroj, N., Abdellatif, M., Kolb, D., Hoeks, J., Kershaw, E. E., Sedej, S., Schrauwen, P., Haemmerle, G., and Zechner, R. (2017) Cold-induced thermogenesis depends on ATGL-mediated lipolysis in cardiac muscle, but not Brown adipose tissue. *Cell Metab.* **26**, 753–763.e7
41. Abdellatif, M., Leite, S., Alaa, M., Oliveira-Pinto, J., Tavares-Silva, M., Fontoura, D., Falcão-Pires, I., Leite-Moreira, A. F., and Lourenço, A. P. (2016) Spectral transfer function analysis of respiratory hemodynamic fluctuations predicts end-diastolic stiffness in preserved ejection fraction heart failure. *Am. J. Physiol. Heart Circ. Physiol.* **310**, H4–H13
42. Moody, G. B. Spectral analysis of heart rate without resampling, IEEE Conference Publication
43. Folch, J., Lees, M., and Sloane Stanley, G. H. (1957) A simple method for the isolation and purification of total lipides from animal tissues. *J. Biol. Chem.* **226**, 497–509
44. Knittelfelder, O. L., Weberhofer, B. P., Eichmann, T. O., Kohlwein, S. D., and Rechberger, G. N. (2014) A versatile ultra-high performance LC-MS method for lipid profiling. *J. Chromatogr. B Analyt. Technol. Biomed. Life Sci.* **951–952**, 119–128
45. Hartler, J., Trötzmüller, M., Chitraju, C., Spener, F., Köfeler, H. C., and Thallinger, G. G. (2011) Lipid Data Analyzer: unattended identification and quantitation of lipids in LC-MS data. *Bioinformatics* **27**, 572–577
46. Särkioja, T., and Hirvonen, J. (1984) Causes of sudden unexpected deaths in young and middle-aged persons. *Forensic Sci. Int.* **24**, 247–261
47. Prichard, B. N., Owens, C. W., Smith, C. C., and Walden, R. J. (1991) Heart and catecholamines. *Acta Cardiol.* **46**, 309–322
48. Andreev, S. V., Kobkova, I. D., Bogdanova, N. M., and Kutyreva, T. S. (1978) Noradrenalin and adrenalin content in the human myocardium after accidental and sudden death. *Bull. Exp. Biol. Med.* **86**, 1003–1006
49. Toriumi, K., Mamiya, T., Song, Z., Honjo, T., Watanabe, H., Tanaka, J., Kondo, M., Mouri, A., Kim, H.-C., Nitta, A., Fukushima, T., and Nabeshima, T. (2015) Deletion of SHATI/NAT8L decreases the N-acetylaspartate content in the brain and induces behavioral deficits, which can be ameliorated by administering N-acetylaspartate. *Eur. Neuropsychopharmacol.* **25**, 2108–2117
50. Karaman, S., Barnett, J., Jr., Sykes, G. P., and Delaney, B. (2011) Subchronic oral toxicity assessment of N-acetyl-L-aspartic acid in rats. *Food Chem. Toxicol.* **49**, 155–165
51. Karaman, S., Barnett, J., Sykes, G. P., Hong, B., and Delaney, B. (2011) Two-generation reproductive and developmental toxicity assessment of dietary N-acetyl-L-aspartic acid in rats. *Food Chem. Toxicol.* **49**, 3192–3205
52. Ishihara, H., Asano, T., Tsukuda, K., Katagiri, H., Inukai, K., Anai, M., Kikuchi, M., Yazaki, Y., Miyazaki, J. I., and Oka, Y. (1993) Pancreatic beta cell line MIN6 exhibits characteristics of glucose metabolism and glucose-stimulated insulin secretion similar to those of normal islets. *Diabetologia* **36**, 1139–1145
53. Nakashima, K., Kanda, Y., Hirokawa, Y., Kawasaki, F., Matsuki, M., and Kaku, K. (2009) MIN6 is not a pure beta cell line but a mixed cell line with other pancreatic endocrine hormones. *Endocr. J.* **56**, 45–53
54. Moffett, J. R., Ross, B., Arun, P., Madhavarao, C. N., and Namboodiri, A. M. A. (2007) N-Acetylaspartate in the CNS: from neurodiagnostics to neurobiology. *Prog. Neurobiol.* **81**, 89–131
55. D'Adamo, A. F., and Yatsu, F. M. (1966) ACETATE METABOLISM IN THE NERVOUS SYSTEM. N-ACETYL-l-ASPARTIC ACID AND THE BIOSYNTHESIS OF BRAIN LIPIDS*. *J. Neurochem.* **13**, 961–965
56. MacPherson, R. E. K., Dragos, S. M., Ramos, S., Sutton, C., Frendo-Cumbo, S., Castellani, L., Watt, M. J., Perry, C. G. R., Mutch, D. M., and Wright, D. C. (2016) Reduced ATGL-mediated lipolysis attenuates β-adrenergic-induced AMPK signaling, but not the induction of PKA-targeted genes, in adipocytes and adipose tissue. *Am. J. Physiol. Cell Physiol.* **311**, C269–C276
57. Duncan, R. E., Ahmadian, M., Jaworski, K., Sarkadi-Nagy, E., and Sul, H. S. (2007) Regulation of lipolysis in adipocytes. *Annu. Rev. Nutr.* **27**, 79–101
58. Newsholme, P., and Krause, M. (2012) Nutritional regulation of insulin secretion: implications for diabetes. *Clin. Biochem. Rev.* **33**, 35–47
59. Vangipurapu, J., Stancáková, A., Smith, U., Kuusisto, J., and Laakso, M. (2019) Nine amino acids are associated with decreased insulin secretion and elevated glucose levels in a 7.4-year follow-up study of 5,181 Finnish men. *Diabetes* **68**, 1353–1358

Received for publication June 27, 2018.
Accepted for publication September 10, 2019.